UNIVERSITE D'OTTAWA / UNIVERSITY OF OTTAWA
École des études supérieures/School of Graduate Studies

Title of thesis THE DEFORMATION KINETICS OF A SUPERPLASTIC ZINC-ALUMINIUM ALLOY

Name of candidate LAFORCE, Clément H.

Degree M.A.Sc. Department Mechanical Engineering

Date of defence November 10, 1977

We, the undersigned, certify that we have approved this thesis and that the candidate has defended it successfully.

S.C. Cheng

J.A. Newman

W. Tyson

A.S. Krausz
(Thesis Supervisor)

(Dean of Graduate Studies)

THE DEFORMATION KINETICS OF A SUPERPLASTIC ZINC-ALUMINUM ALLOY

by

Clément H. Laforce

A thesis submitted to the School of Graduate Studies
of the University of Ottawa,
in partial fulfillment of the requirements
for the degree of

MASTER OF APPLIED SCIENCE
IN MECHANICAL ENGINEERING

University of Ottawa,
Ottawa, Ontario, Canada

August 1977

THE DEFORMATION KINETICS OF A SUPERPLASTIC ZINC-ALUMINUM ALLOY

ABSTRACT

The deformation behavior of a commercial near eutectoid zinc-aluminum alloy was studied by subjecting standard tensile specimens to stress relaxation experiments at constant temperatures between 258 ^{0}K to 344 ^{0}K.

To satisfy the constant strain condition of such experiments, the testing machine was controlled by a computer; for comparative purposes, other tests were conducted using the normal stress relaxation procedure.

The results of the experiments were analysed using the theory of deformation kinetics. It was concluded that, for the temperature range covered in this investigation, the deformation mechanisms operate sequentially.

The activation volumes associated with forward activation over the first barrier were measured to be 13 ± 1 b^3; for the forward activation over the second barrier, the activation volumes were found to be 38 ± 14 b^3, while those characteristic to the backward flow over the first barrier varied from 27 to 252 b^3.

It was not possible to obtain accurate measurements of the activation energies; consequently, no conclusion could be drawn as to the nature of

the deformation mechanisms.

The stress exponent, defined as $\partial \ln \dot{\tau} / \partial \ln \tau$, was also measured; the values found varied from 2.1 to 9.3.

ACKNOWLEDGEMENTS

The author would like to express his gratitude to his advisor, Dr. A. S. Krausz, for his help throughout every stage of this project; his suggestions and encouragement were much appreciated.

The long discussions with Dr. W. H. Ginman and Mr. B. Faucher, whose insights into the finer points of experimental techniques and theoretical formulation prevented many mistakes, are gratefully recognized.

Much indebtedness is also owed to Messrs. D. Seaman, G. Toth, O. Dalnoki, G. Spak, J. Zika and M. Makasare for their technical assistance and their constant willingness to meet the often impossible deadlines requested by the author.

The struggle for a better understanding of the theoretical knowledge was shared by the author's lab partner, Miss M. Akben, whose patience and suggestions were invaluable.

The financial assistance provided by the Government of Ontario through its Graduate Scholarship Program is acknowledged. Many thanks are due to the Research Centre of Noranda Metal Industries Ltd., who supplied the specimen material.

Finally, the author would like to express his love and recognition to the members of his family for their encouragement during this work.

TABLE OF CONTENTS

LIST OF FIGURES

LIST OF TABLES

NOMENCLATURE

b	Burgers vector
h	Planck's constant
k	Boltzmann's constant
m	limit for counter
n	limit for counter; stress exponent
t	time
k	rate constant
A	preexponential factor in rate equation
E	Young's modulus
E'	combined elastic modulus
ΔE	activation energy
ΔG	Gibbs free energy
K	machine stiffness; proportionality constant in control program
L	length
R	shear stress rate
T	temperature
V	activation volume
W	work
δ	contribution of one activation to the deformation
ε	normal strain

κ transmission coefficient

ρ flow unit density

σ normal stress

τ shear stress

Δ change of

Σ summation of

Superscripts

$\ddagger$ activated state

$\cdot$ differentiation w.r.t. time

numerals- see note

Subscripts

a applied; counter in control program

e elastic

i internal; counter in control program

j counter in control program

m machine

o initial

p plastic

t total; true

eff effective

numerals- see note

NOTE:

The rate constants, preexponential factors, activation energies, and activation volumes are labelled as, for example, ${}_{i}k^{j}$ or ${}^{j}k_{i}$, where i represents the reactant state and j the product state. The numerals i and j are arranged as ${}_{i}k^{j}$ in the case of forward activation and as ${}^{j}k_{i}$ in the case of backward activation.

THE DEFORMATION KINETICS OF A SUPERPLASTIC ZINC-ALUMINUM ALLOY

CHAPTER 1

INTRODUCTION AND THEORY

1.1 INTRODUCTION

Superplasticity is a relatively new phenomenon in materials science; it is, as its name implies, a state of some materials in which they exhibit an abnormally extended ductility at low stresses and temperatures. A common example of superplasticity is the deformation behavior of a heated glass rod which can be stretched to many times its original length without breaking.

Jenkins was the first to report on superplastic effects in metals in 1928; six years later, Pearson presented detailed observations on the behavior of a eutectic Bi-Sn alloy that was stretched to nearly 2000% before fracture. Further investigations were reported in 1945 by Bochvar and Sviderskaia and in the late fifties by Presnyakov and co-workers, who studied the behavior of eutectic or eutectoid systems in alloys of Al-Zn, Al-Cu, Al-Si, Al-Ni, Al-Fe, Cu-Zn and Cu-Ni. Following the work of Backofen et al. in the early sixties, considerable interest in the subject was stirred and since then, numerous studies of superplastic phenomena have been reported. [1,2,3]

Superplastic materials are generally divided in two distinct types; the first group exhibits structural superplasticity. Such alloys are often, though not always, of eutectic or eutectoid composition. Superplastic behavior in this category has been closely linked to a stable, equiaxed grain structure, where the grains are typically less than 10 micrometers in diameter. Further restrictions on the occurrence of such behavior include a forming temperature from 0.4 to 0.5 of the alloy's absolute melting temperature, and a specific range of strain rates.

The second type of superplasticity is produced by repeated temperature cycling through a phase transformation, or by temperature cycling of thermally anisotropic materials, or by neutron irradiation.[1] Such superplastic behavior is called environmental and will not be discussed in greater depth; further reference to the term superplasticity will relate to the first type.

There have been few large scale applications of superplasticity in industry. Pressure forming techniques have been used to demonstrate the forming of complex parts and, though the power requirements are low (superplasticity occurs at low stresses), the strain rates needed to preserve superplasticity are too low, making the operation too lengthy to be economical. A further disadvantage is the need to give the finished parts a heat treatment to destroy the superplastic state.

The purpose of this investigation was to study the deformation behavior of a commercial near-eutectoid zinc-aluminum alloy manufactured by Noranda Mines Ltd. under the trade name of Z-500.[3,5]

Z-500 is marketed as a free-cutting alloy mainly for screw machining purposes. It is a zinc base quaternary alloy composed of 25% by weight of aluminum, 5% of copper and 0.05% of magnesium. Its mechanical and physical properties are presented in Appendix 1. Z-500 behaves superplastically from 200 ^{0}C to 275 ^{0}C.

The research involved subjecting standard tensile specimens to stress relaxation experiments at near-room temperatures. The results were analysed with the theory of deformation kinetics.[6]

This report is divided into four chapters; the basic theoretical relationships are established in the first. Chapter 2 describes the experimental and testing procedures, while the methods used to analyse the data are explained in Chapter 3. The last chapter contains the discussions and conclusions.

1.2 THE THEORY OF DEFORMATION KINETICS

A good understanding of plastic deformation is of primary importance to the manufacturing engineer. This understanding can be promoted by viewing a solid as a giant molecule. Within this molecule, the atoms vibrate about their equilibrium positions or free energy wells (Figure 1.2.1). Upon application of stress, the atoms are displaced from their equilibrium positions; added to this displacement, the random thermal agitation makes it possible that at a given time, the atom or group of atoms will possess enough energy to surmount the energy barrier and move into another energy well. In this process,

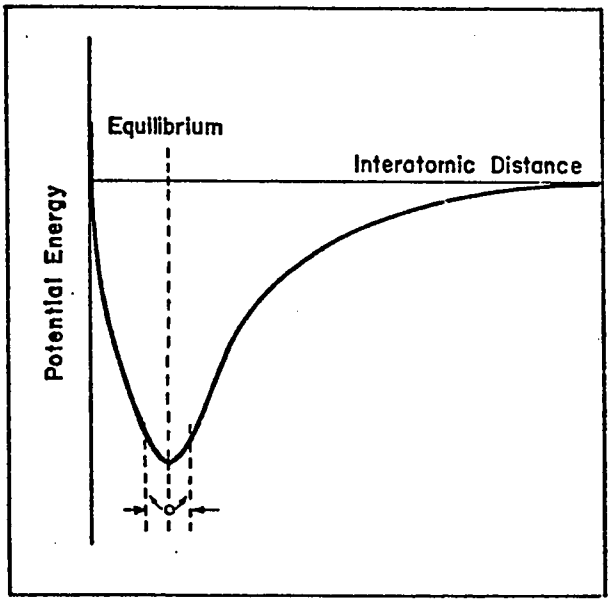

Figure 1.2.1 The potential energy vs interatomic distance relation between two atoms, showing the energy well about which the atoms vibrate. In a solid, the energy well is repeated at each atom.

bonds are broken and new ones created, thus changing the structure of the solid, or molecule. A sufficient number of such events, called thermal activations, results in a permanent, macroscopic change in the shape of the solid. It should then be obvious that plastic deformation is a process analogous to the isomerization of the giant molecule, the specimen.

The basic statement of deformation kinetics is that the nature of plastic deformation is indistinguishable from that of chemical reactions and that the concepts and theories of chemical kinetics are applicable to the description of deformation processes.

The first assumption made is that the reacting system is in equilibrium; in other words, the proportion between reacting complexes, those that have enough energy to surmount the energy barrier, and the ordinary, non-reacting complexes is constant. This assumption leads to the basic equation of kinetic theory:[6] the rate of a simple chemical reaction is controlled by a rate constant, k, expressed as

$$k = A_e \exp\left(\frac{-\Delta E_e}{kT}\right) \qquad (1.2.1)$$

where A_e is a frequency factor and ΔE_e an activation energy; k is Boltzmann's constant and T the absolute temperature.

The above equation describes empirically the rate of a simple process where activation proceeds in one direction over a single energy barrier. However, this is not applicable to the general case. Plastic

deformation may occur in separate, distinct steps. The remainder of this section will establish the necessary relationships for the analysis of the experimental results. The development of these will be non-rigorous as a full treatment would be out of the scope of this project.

ACTIVATION OVER A SINGLE ENERGY BARRIER

Plastic deformation occurs when a reacting complex acquires enough energy to overcome an energy barrier. The simplest case one can consider is that of a single energy barrier as shown in Figure 1.2.2. Since any solid is composed of a great number of atoms, a true representation of the surface describing the full energy relationship among all atoms will require a correspondingly larger number of dimensions. Figure 1.2.2 represents the most probable path the reacting complex might take. The top of the barrier is called the activated state, indicated by the symbol $\ddagger$; it is, by definition, a saddle point. A complex having enough energy

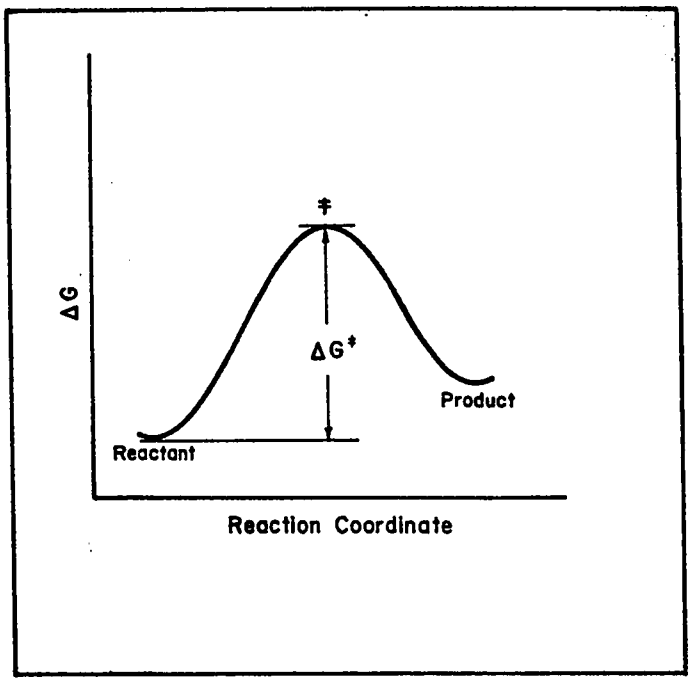

Figure 1.2.2 The representation of a single energy barrier.

to reach this level is thus most likely to proceed to the final, or product state.

Eyring [6] has shown theoretically that the rate constant of the flow over this barrier can be expressed as

$$k^{\ddagger} = \kappa \frac{kT}{h} \exp\left(\frac{-\Delta G^{\ddagger}}{kT}\right) \qquad (1.2.2)$$

where κ is the transmission coefficient, a measure of the fraction of complexes that are reflected back from the activated state or tunnel through the energy barrier; h is Planck's constant and $\Delta G^{\ddagger}$ is the difference in Gibbs free energy from the reactant state to the activated state. For low temperature deformation of metals, the transmission coefficient is unity.

When stress is applied, the effective height of the barrier in the forward direction is decreased as shown in Figure 1.2.3 [6]. This figure also shows that activation is not restricted to forward movement but can also proceed in the reverse direction, against the applied stress. The rate constant in the forward direction is then rewritten as

$$_1k^1 = \frac{kT}{h} \exp\left(-\frac{_1\Delta G^{1\ddagger} - {}_1W^1}{kT}\right) \qquad (1.2.3)$$

where W is a work term, a function of the stress τ. This relationship will be expressed as $W = V\tau$, where V is the activation volume. The activation volume is related to the complex that undergoes activation; as such, it is an indication of the mechanism that controls the plastic flow.

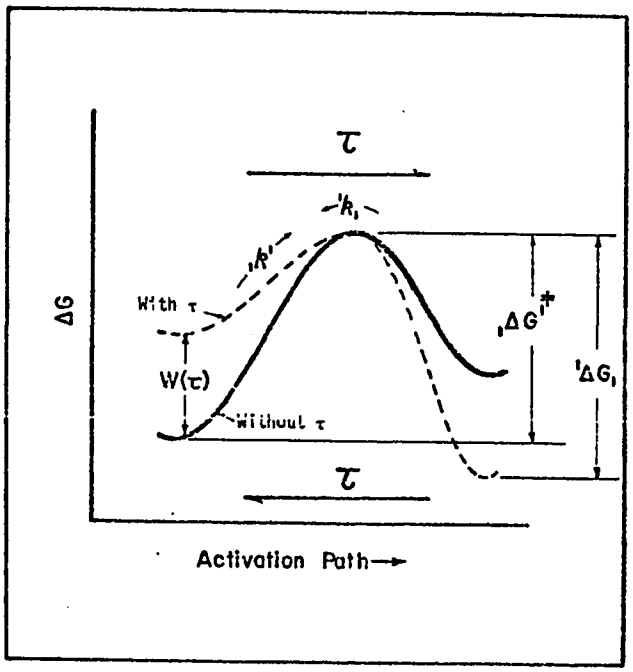

Figure 1.2.3 The effect of stress on the shape of the energy barrier. The figure also shows the rate constants identified with their proper notation.

Similarly, the backward rate constant is expressed as

$$ {}^1k_1 = \frac{kT}{h} \exp\left(- \frac{{}^1\Delta G^{\ddagger}_1 + {}^1W_1}{kT} \right) \qquad (1.2.4) $$

The overall rate constant is then the difference between the two elementary constants, namely

$$ k = {}_1k^1 - {}^1k_1 \qquad (1.2.5) $$

Finally, the deformation rate is obtained by multiplying the rate constants by the concentration of flow units, ρ, and by the contribution to the rate of each activation, δ, as

$$\text{Rate} = R = \delta\rho({}_1k^1 - {}^1k_1) \tag{1.2.6}$$

The flow units are generally considered to be the crystalline defects that cause plastic flow; these may be vacancies, interstitial atoms, or mobile dislocations. The atoms lying along these imperfections are far out of equilibrium and consequently are more apt to migrate under the influence of stress.

ACTIVATION OVER A SYSTEM OF ENERGY BARRIERS

As mentioned previously, deformation processes do not generally occur by activation over one energy barrier. Plastic flow can depend on different mechanisms which may form either a parallel or consecutive system or a combination of both.

Considering m independent processes (Figure 1.2.4), the rate over the first barrier is, as before

$$R_1 = \delta_1 \rho_1 ({}_1k^1 - {}^1k_1)$$

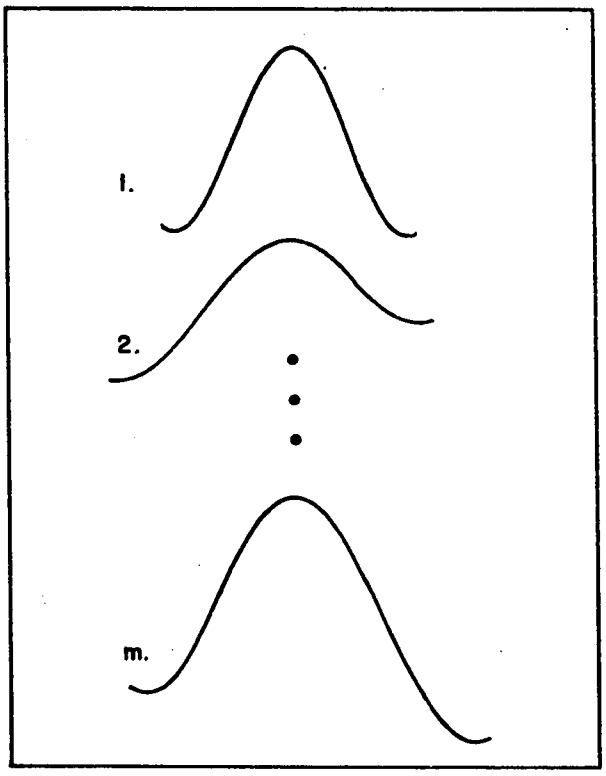

Figure 1.2.4 A parallel system of m energy barriers.

and over the j-th barrier

$$R_j = \delta_j \rho_j ({}_jk^j - {}^jk_j)$$

The overall rate is just the sum of each individual rate, i.e.

$$R = \sum_{j=1}^{m} R_j = \sum_{j=1}^{m} \delta_j \rho_j ({}_jk^j - {}^jk_j) \qquad (1.2.7)$$

The expression for consecutive processes will be derived for a system of two barriers only, as shown in Figure 1.2.5.

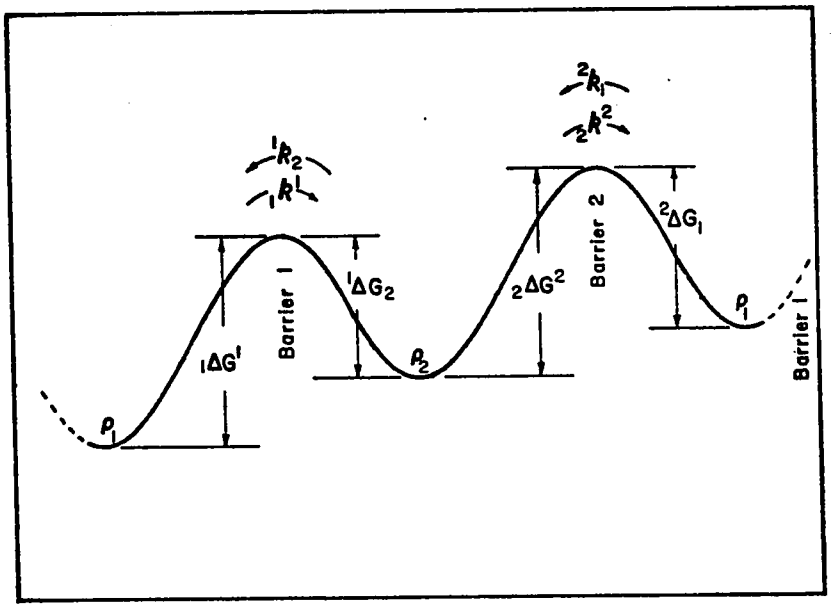

Figure 1.2.5 A system of two consecutive energy barriers. The figure also shows the repetitive pattern of this system.

Considering a total concentration ρ_t of flow units held up in either valley, it follows that

$$\rho_1 + \rho_2 = \rho_t \tag{1.2.8}$$

In steady state conditions, ρ_1, ρ_2 and ρ_t remain unchanged in time; consequently, the net flow into valley 2 is equal to that leaving it. Using the notation of Figure 1.2.5, we find

$$\rho_{11}k^1 + \rho_1{}^2k_1 = \rho_2{}^1k_2 + \rho_{22}k^2 \tag{1.2.9}$$

where each rate constant is of the form

$$k = \frac{kT}{h} \exp\left(-\frac{\Delta G^{\ddagger} \pm W}{kT}\right)$$

Substituting for ρ_2 from Eq. (1.2.8) into Eq. (1.2.9) and rearranging

$$\rho_1 = \rho_t \frac{{}^1k_2 + {}_2k^2}{{}_1k^1 + {}_2k^2 + {}^2k_1 + {}^1k_2} \tag{1.2.10}$$

The net rate over barrier 2 is

$$R = \delta(\rho_{22}k^2 - \rho_1{}^2k_1) \tag{1.2.11}$$

Again substituting for ρ_2

$$R = \delta\{\rho_{t2}k^2 - \rho_1({}_2k^2 + {}^2k_1)\} \tag{1.2.12}$$

Using the expression for ρ_1 in Eq. (1.2.10) and substituting in Eq. (1.2.12)

$$R = \delta\rho_t\left\{{}_2k^2 - \frac{({}^1k_2 + {}_2k^2)({}^2k_1 + {}_2k^2)}{{}_1k^1 + {}_2k^2 + {}^2k_1 + {}^1k_2}\right\}$$

$$= \delta\rho_t \frac{{}_2k^2{}_1k^1 - {}^2k_1{}^1k_2}{{}_1k^1 + {}_2k^2 + {}^2k_1 + {}^1k_2} \tag{1.2.13}$$

Finally, Eq. (1.2.13) is reorganized as

$$R = \delta\rho_t \frac{1 - \frac{{}^2k_1\,{}^1k_2}{{}_1k^1\,{}_2k^2}}{\frac{1}{{}_1k^1} + \frac{1}{{}_2k^2} + \frac{{}^1k_2}{{}_1k^1\,{}_2k^2} + \frac{{}^2k_1}{{}_1k^1\,{}_2k^2}} \qquad (1.2.14)$$

And thus, as derived in Appendix 2:

$$R = \delta\rho_t \frac{kT}{h} \frac{1 - \exp\left(\frac{{}^1\Delta G_1}{kT}\right)}{\exp\left(\frac{{}_1\Delta G^1}{kT}\right) + \exp\left(\frac{{}_2\Delta G^2}{kT}\right) + \exp\left(\frac{{}_1\Delta G^2}{kT}\right) + \exp\left(\frac{{}_2\Delta G^1}{kT}\right)} \qquad (1.2.15)$$

This same analysis can be taken to any level of complexity, depending on the system of barriers. The proper combination of parallel/series expressions can then describe any deformation process.

Experimental evaluation of the kinetics of a deformation process must always be done in such a way that the simplest combination of elementary rate constants match the observed behavior. The parameters obtained from this analysis must then be examined for physical significance; only then can meaningful conclusions on the nature of the operating mechanisms be made.

1.3 STRESS RELAXATION: DEFORMATION AT CONSTANT STRAIN

The deformation of a material depends on many variables, namely stress, strain, rate of loading, structure and previous deformation history. A good testing procedure allows one quantity to vary while controlling the behavior of the others.

A stress relaxation experiment is one in which the total strain in the specimen is not allowed to change. Its purpose is to study the variation of stress with respect to time. Furthermore, the total deformation during the test being small, structural changes in the material are kept to a minimum.

The usual procedure is to load a specimen at a constant rate to a pre-determined stress, normally past the elastic limit and then to stop the crosshead of the machine, subsequently recording the load. This is illustrated in Figure 1.3.1.

After some time, the load will no longer change; the stress at this level is called the internal stress, indicated by the subscript i. This internal stress results from the forces exerted by the atoms lying in non-equilibrium positions along crystalline flaws. A discussion on the method of determination of the internal stress is included in Chapter 2.

Some of the first stress relaxation experiments reported are those of

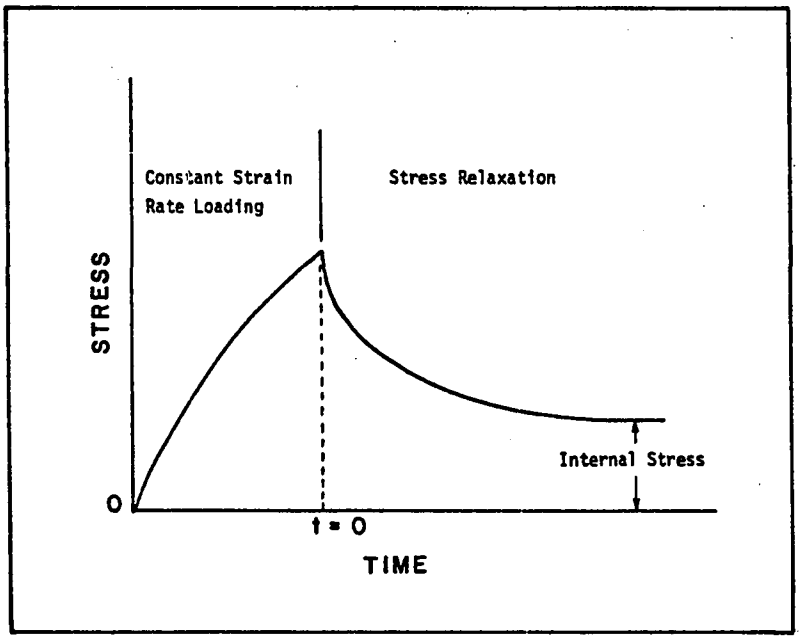

Figure 1.3.1 A schematic representation of a stress relaxation experiment.

Trouton and Rankine, [6] who used a different method. A long specimen was subjected to a constant load; after the specimen had elongated a pre-determined strain ε_t (in this case 3×10^{-7}), the load was decreased so that the specimen contracted to $-\varepsilon_t$. This was repeated a number of times, the relaxation experiment then being approximated by a series of oscillating creep tests.

Since then, the majority of stress relaxation tests follow the first method described, with the restriction that the machine used be so rigid as to render negligible any deflections occuring during relaxation.

CHAPTER 2

EXPERIMENTAL PROCEDURE

One of the minor goals of this investigations was to study the performance of a numerical control system built in the department.[7] To do so, three different relaxation techniques were used; eleven tests were performed on a modified Hounsfield tensometer with the numerical control; in addition, nine tests were conducted on the same machine without the control and finally, five experiments were done on a model TTC-M Instron tensile testing machine.

2.1 THE HOUNSFIELD TENSOMETER

The Hounsfield tensometer is a soft machine; the load measuring device consists of a flat beam supported at both ends and which can deflect as much as 0.8 mm at full scale loading. When doing a stress relaxation experiment, the normal procedure where the crosshead is simply fixed does not ensure that the total strain during the test remains negligible. The deflection of the spring beam during a normal load reduction induced as much as 1.3% strain in the specimen. This, added to the deflections of the machine frame itself, makes the machine too soft to perform true stress relaxation experiments.

The tensometer had been previously modified to make it compatible with the control system. The manual loading device was replaced by a synchronous stepping motor which, through a gear reduction, produced a crosshead displacement of 1/60 of one thousandth of one inch per step. The load cell was also fitted with a linear variable differential transducer (Hewlett Packard 7DCDT-050) which provided an analog signal for load.

The control system constantly monitored the length of the specimen and when its change exceeded some prescribed limit $\Delta\varepsilon_t$, the system would activate the stepping motor and move the crosshead the required distance to bring back the specimen's length within limits. This procedure results in a stepwise relaxation similar to that used by Trouton and Rankine (sect. 1.3). This is illustrated schematically in Figure 2.1.1, along with the normal, hard-machine relaxation procedure.

A component-by-component description of the control system, as well as a flowchart and control program, are included in Appendix 4.

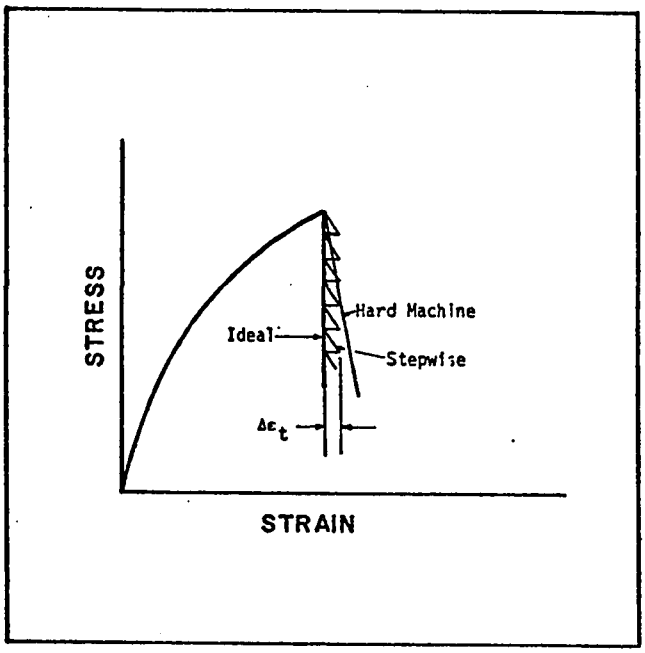

Figure 2.1.1 A schematic illustration of the difference between controlled and normal stress relaxation procedures.

2.2 THE INSTRON UNIVERSAL TESTING INSTRUMENT

The Instron tensile testing machine is designed for scientific applications; the machine is often used by researchers in materials science. Its rigidity and accuracy made it an obvious choice to compare the results of the experiments done on the Hounsfield tensometer.

The experiments were carried out without the control system; the behavior of the specimens was similar to that of those tested on the Hounsfield, with the exception that the specimens deformed approximately half the amount they would have on the Hounsfield without the control. A discussion of the differences in behavior when using this machine is included in Chapter 4.

2.3 EXTENSOMETRY AND TEMPERATURE CONTROL

Three of the eleven tests with the numerical control (specimens #6, 8 and 17) were performed with a grip-mounted strain gauge (Hewlett Packard 7DCDT-100 linear variable differential transducer); this system is suitable when the duration of the test is short; i.e., when the stress is high enough to render grip slipping negligible.

For the other experiments, a specimen-mounted extensometer was used (Instron G51-12 or G51-11MA). This method has the advantage of monitoring the true length changes in the specimen and is thus more suitable for the control system. The control limit ($\Delta\varepsilon_t$ in Figure 2.1.1) was set at 4.8×10^{-5} strain during the controlled tests.

Most of the room temperature experiments were conducted without temperature control. The tensometer was placed in an insulated enclosure and the temperature was allowed to reach steady state before testing began. For the higher temperature tests, the air temperature was increased by a space heater with a built-in thermostatic control. The set-up was similar for the lower temperature experiments. The tensometer, inside two foam enclosures, was placed in a refrigerated room.

The temperature was measured by thermocouples which indicated differences of $\pm 0.5\ ^0K$ for most tests and $\pm 1.0\ ^0K$ for all. No measurable temperature difference was noted along the length of the specimen.

These temperature fluctuations were found to have negligible effects on the values of the activation parameters; also, the thermal expansion of the material under these conditions produced a strain which was well within the control limits.

2.4 GENERAL TESTING PROCEDURE

The specimens (Figure 2.4.1) were first mounted on the machine; the extensometer was attached to the specimen and aligned. The tensometer was then isolated and the temperature allowed to settle. The specimen was loaded at a constant rate to a stress level between the yield stress and the ultimate tensile strength; at that point, the crosshead was stopped and, for the tests with control, the system was activated. The load change was recorded on a Hewlett Packard Model 9100B strip chart recorder. The temperature was also recorded for most specimens as well as the length, for ten specimens. A typical relaxation curve is shown in Figure 2.4.2.

Most of the load relaxation occured within a few hours but the time needed for it to level off was much greater, especially at lower temperatures; the tests generally lasted several days. One experiment lasted 48 days (specimen #25) and it was found that the information gained did

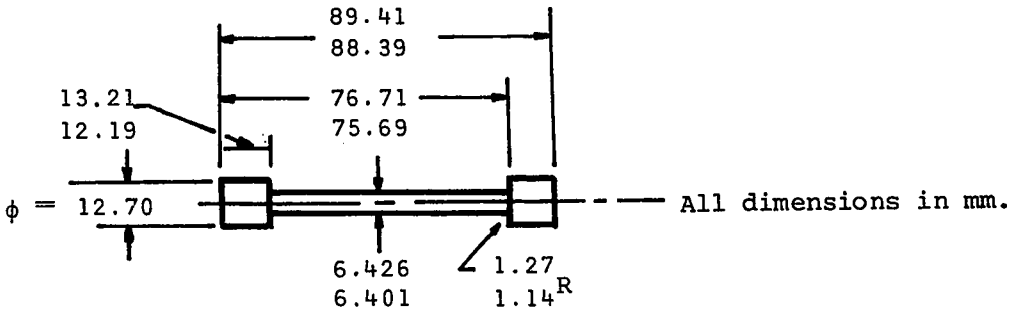

Figure 2.4.1 The specimens used for the relaxation experiments.

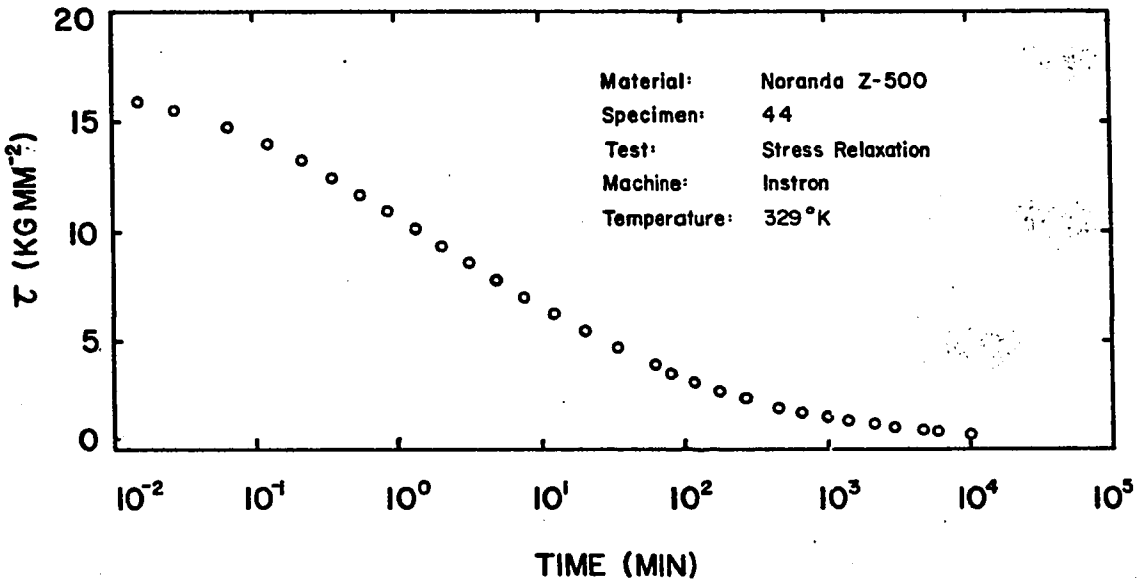

Figure 2.4.2 A relaxation curve for an initial stress, τ_o, of 16.45 kg/mm^2.

not warrant the extra time and effort; some other tests were cut short because of experimental mishaps such as equipment failure. The initial portion of these tests was nevertheless useful and was included in this report. Table 2.4.1 describes each experiment.

The times for specimens #30 and #34 are not listed there. For these two tests, a different procedure was used: the specimens were loaded as usual and relaxation was allowed to proceed without control for two days. The load was then decreased instantaneously by a small amount, followed by several hours of relaxation. This was repeated a number of times. The reason for this was to obtain the rates of load change at low stresses without having to wait the long periods of time it would normally have taken. The data thus obtained was not compatible with the algorithm used

TABLE 2.4.1 THE DESCRIPTION OF THE EXPERIMENTS

	SPECIMEN	MACHINE	τ_o (kg/mm^2)	τ_i (kg/mm^2)	TIME (min/day)	TEMPERATURE (^{0}K)
1	C	Hounsfield No Control	16.45	3.00	15000 / 10	300
2	D	"	18.45	2.50	10000 / 7	300
3	6	Hounsfield Controlled	16.15	1.80	1400 / 1	300
4	8	"	18.05	2.50	600 / 0.5	300
5	9	Instron	17.50	2.00	4900 / 3.5	301
6	15	Hounsfield Controlled	17.45	1.75	1000 / 1	300
7	17	"	17.85	2.30	500 / 0.5	300
8	18	"	18.40	1.25	8500 / 6	300
9	22	"	20.50	1.50	35000 / 24	300
10	23	"	19.85	1.10	20000 / 14	300
11	25	"	19.60	0.70	70000 / 48	300
12	27	"	17.80	2.00	2000 / 1.5	300
13	28	"	19.20	2.00	1400 / 1	300
14	29	"	19.10	0.80	8000 / 6	300
15	30	Hounsfield No Control	19.35	0.70	----------	308
16	34	"	22.55	2.80	----------	284
17	36	Instron	21.50	5.65	4300 / 3	280
18	37	Hounsfield No Control	13.75	0.35	2100 / 1.5	344
19	38	Instron	23.50	8.05	11700 / 8	258
20	39	Hounsfield No Control	16.40	0.80	8000 / 6	327
21	40	"	17.00	0.60	11450 / 8	330
22	41	Instron	17.45	0.45	14350 / 10	338
23	42	Hounsfield No Control	17.30	0.65	15500 / 11	329
24	43	"	17.45	1.10	12750 / 9	317
25	44	Instron	16.45	0.65	10000 / 7	329

to measure rates (see Chapter 3 and Appendix 3), and graphical differentiation at very low stresses is not applicable. Consequently, this method was judged unsatisfactory and was not repeated.

THE MEASUREMENT OF THE INTERNAL STRESS

Internal stresses are those created by the non-equilibrium atoms within a solid; the true, effective stress, τ_{eff}, that causes plastic flow is a function of this internal stress and is defined as

$$\tau_{eff} = \tau_a - \tau_i \qquad (2.4.1)$$

where τ_a is the applied stress and τ_i is the internal stress.

Deformation ceases when the effective stress is zero, or when the applied stress equals the internal stress. The determination of the internal stress is quite important in kinetics as the required value in the analysis is the effective stress. Gibbs [8] proposed the following method to determine the internal stress.

When a relaxing specimen is suddenly unloaded to a stress lower than its internal stress, it undergoes a process called negative relaxation where the load increases in time as shown in Figure 2.4.3. A series of positive and negative relaxation "tests" eventually sets a range for the internal stress.

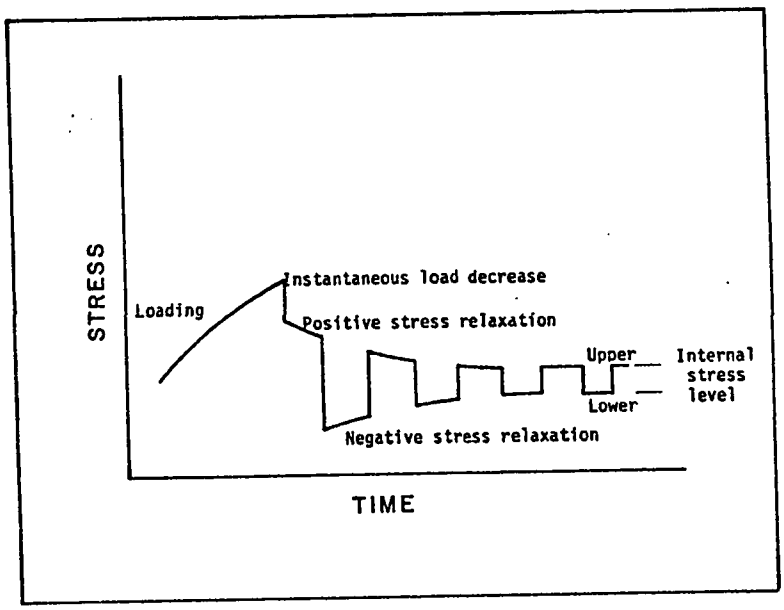

Figure 2.4.3 A schematic representation of the method used to determine the internal stress level (from Reference 6).

The internal stresses reported in Table 2.4.1 are the average values of the range defined by this procedure. In the cases where experimental difficulties prevented this measurement, the internal stresses were determined from an extrapolation of the stress versus logarithm of time plots.

CHAPTER 3

THE ANALYSIS OF THE DEFORMATION PROCESSES

The analysis of the kinetics of a process is carried out in an orderly manner; the simplest mathematical representation possible is first fitted to the data and then more complex functions are systematically matched until the experimental results are fully described. The mathematical evaluation will then yield parameters that must be scrutinized for their physical significance; this includes rejecting interpretations that lead to physical impossibilities and comparing the others to established theoretical or experimental values. (9)

A kinetics analysis expresses the effect of stress and temperature on deformation rate; this eventually leads to a better comprehension of the rate-controlling mechanisms and, since the first step in controlling a process is understanding it, the information thus gained is ultimately of great interest.

The results of such investigations are usually depicted in a semi-logarithmic plot as logarithm of deformation rate versus stress; in this system, the exponential dependence of rate on stress becomes linear and complex processes which are controlled by several mechanisms appear as some combination of each individual linear relationship.

3.1 THE DEFORMATION KINETICS

The first step in the analysis was to calculate the stress rates; this was done initially by graphical differentiation of the stress versus time output from the strip chart recorder. A numerical method to obtain the rates was then used and its results were compared with those obtained from the graphical method; the relative error between the two methods was found to be less than 1% for all points. Since the numerical differentiation method provided a more objective way to evaluate the data, it was applied for all experiments. This method is briefly described in Appendix 3.

A typical rate diagram is presented in Figure 3.1.1. The linear behavior in the higher stress zone indicated that, at that level, the deformation process was controlled by forward activation over a single energy barrier. Rewriting Eq. (1.2.3) in terms of stress rate and substituting the expression for the work term, we find

$$R = \delta\rho_1 A^1 \exp\left(\frac{{}_1V^1\tau_{eff}}{kT}\right) \qquad (3.1.1)$$

A line of this form then yielded the parameters ${}_1V^1/kT$ as slope and $\ln(\delta\rho_1 A^1)$ as intercept, where ${}_1A^1 = \frac{kT}{h}\exp(-{}_1\Delta G^{\mp 1}/kT)$ (*). This is indicated in Figure 3.1.2.

* - The method used to fit the curves to the data is described in Appendix 3.

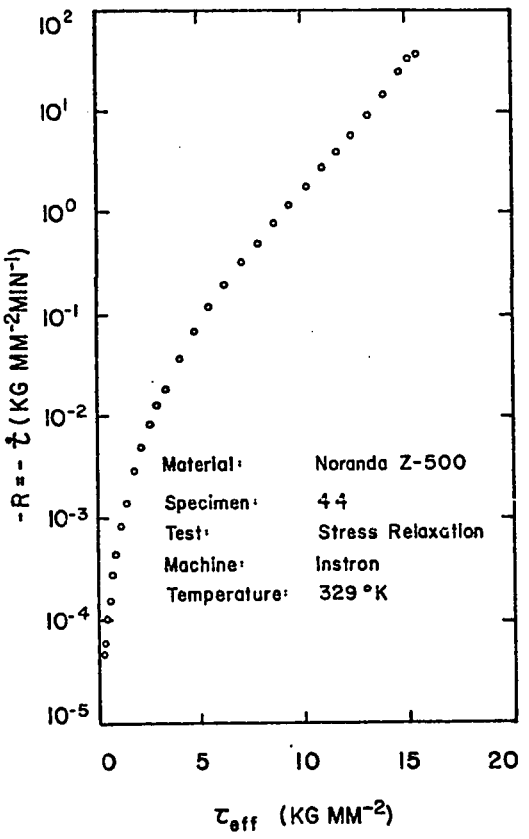

Figure 3.1.1 A typical rate diagram.

At lower stresses, the data fall below the line described above. This behavior is indicative of a retarding mechanism (i.e., either backward activation over the first barrier or forward activation over a second, consecutive barrier). A parallel process would contribute an extra quantity to the rate and the data points would lie above the line.

The possibility that activation could proceed against the applied stress was then investigated. The functional representation of this

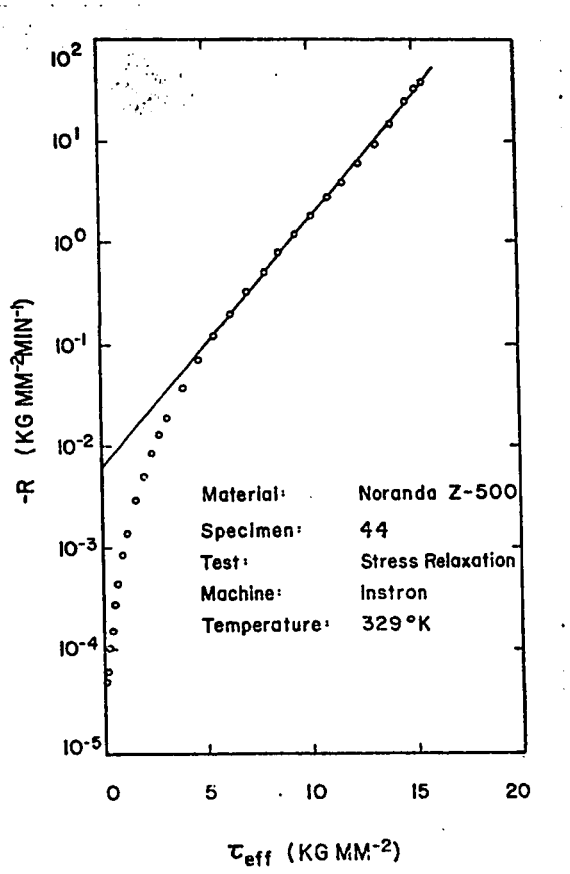

Figure 3.1.2 The result of the analysis for the first term.

system is

$$R = \delta\rho_1 A^1 \exp\left(\frac{{}^1V^1\tau_{eff}}{kT}\right) - \delta\rho^1 A_1 \exp\left(\frac{-{}^1V_1\tau_{eff}}{kT}\right) \qquad (3.1.2)$$

or

$$\delta\rho_1 k^1 - R = \delta\rho^1 A_1 \exp\left(\frac{-{}^1V_1\tau_{eff}}{kT}\right) \qquad (3.1.3)$$

Since $\delta\rho_1 k^1$ is known from the previous analysis, a plot of ln $(\delta\rho_1 k^1 - R)$ versus τ_{eff} should yield points describing a line of negative slope. As can be seen from Figure 3.1.3, this is not so. The data from various

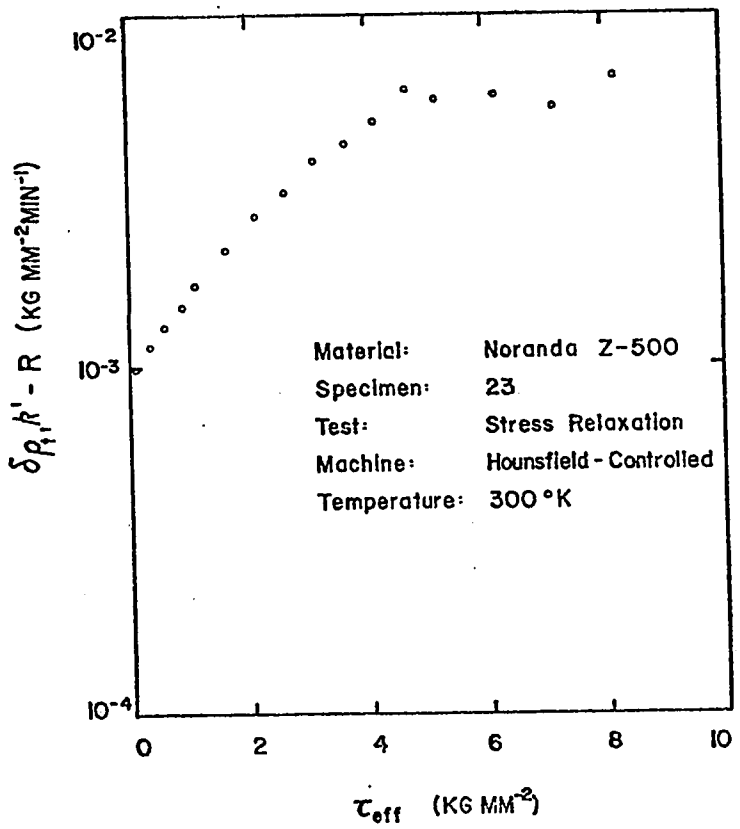

Figure 3.1.3 The analysis for the backward term over the first barrier.

tests was examined in this manner and in none of the cases was there a sufficiently long straight line to justify the assumption.

It was then concluded that the processes occurred in a sequential manner. The equation describing the flow over a system of two consecutive barriers was established in section 1.2 as

$$R = \delta\rho_t \frac{1 - \dfrac{{}^2k_1\,{}^1k_2}{{}_1k^1\,{}_2k^2}}{\dfrac{1}{{}_1k^1} + \dfrac{1}{{}_2k^2} + \dfrac{{}^1k_2}{{}_1k^1\,{}_2k^2} + \dfrac{{}^2k_1}{{}_1k^1\,{}_2k^2}} \qquad (3.1.4)$$

The second term in the numerator represents backward activation over the two barriers (Appendix 2) and can be safely ignored at high stresses. Similarly, the last two terms of the denominator are functions of backward activation over each of the two barriers and generally would not show up at this stage of the analysis. Eq. (3.1.4) was then rewritten as

$$R = \frac{\delta\rho_t}{\frac{1}{{}_1k^1} + \frac{1}{{}_2k^2}} \qquad (3.1.5)$$

which is rearranged

$$\frac{\delta\rho_{t1}k^1R}{\delta\rho_{t1}k^1 - R} = \delta\rho_{t2}k^2 = \delta\rho_{t2}A^2 \exp\left(\frac{{}_2V^2\tau_{eff}}{kT}\right) \qquad (3.1.6)$$

The experimental data was then plotted in the $\ln\left(\frac{\delta\rho_{t1}k^1R}{\delta\rho_{t1}k^1 - R}\right)$ versus τ_{eff} system (Figure 3.1.4). A line was fitted through the points as shown and the parameters $\ln(\delta\rho_{t2}A^2)$ and ${}_2V^2/kT$ were obtained.

As can be seen from Figure 3.1.4, the two-term expression of Eq. (3.1.5) did not fully match the observed behavior; an attempt was made to include in the analysis the second term of the numerator of Eq. (3.1.4), but this formulation did not agree with the data. Adding a single backward term to the rate equation, we get

$$R = \frac{\delta\rho_t}{\frac{1}{{}_1k^1} + \frac{1}{{}_2k^2} + \frac{{}^1k_2}{{}_1k^1{}_2k^2}} \qquad (3.1.7)$$

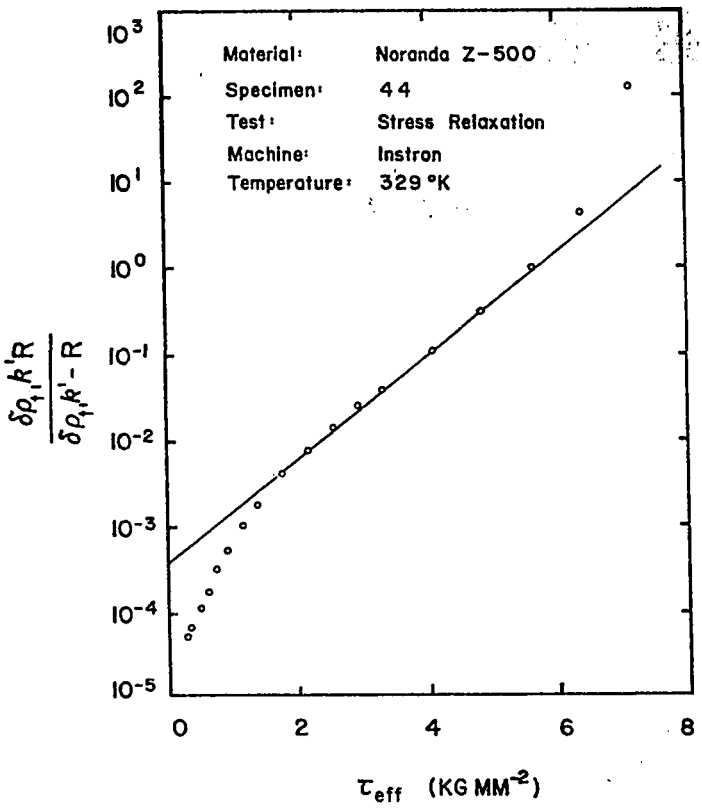

Figure 3.1.4 A typical example of the analysis for the second term, $_2k^2$.

Equation (3.1.7) was rearranged in order to isolate the new term

$$\delta\rho_t\{ \frac{\delta\rho_{t1}k^1{}_2k^2}{R} - {}_1k^1 - {}_2k^2 \} = \delta\rho_t{}^1k_2 = \delta\rho_t{}^1A_2 \exp\left(-\frac{{}^1V_2\tau_{eff}}{kT}\right) \quad (3.1.8)$$

In the $\ln\{ \delta\rho_t(\frac{\delta\rho_{t1}k^1{}_2k^2}{R} - {}_1k^1 - {}_2k^2)\}$ versus τ_{eff} coordinate system, the data should fit a straight line of negative slope. This is shown in Figure 3.1.5.

This fully represented the data and consequently the analysis was not carried out any further. Only six tests were of sufficiently long duration to exhibit the full three terms. Since the rate depends strongly

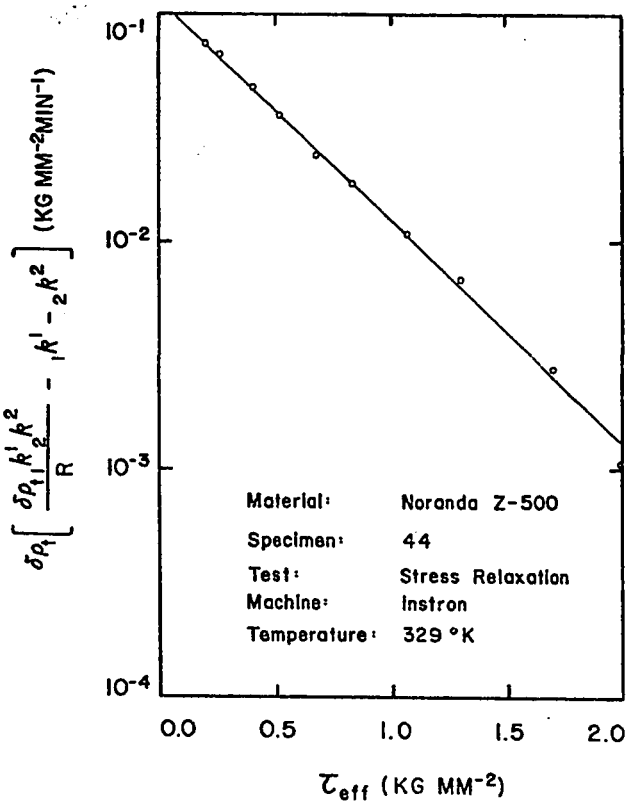

Figure 3.1.5 The analysis for the third term.

on the temperature, none of the tests performed at below-room temperatures showed more than the first term; also, only one of the experiments carried out at room temperature displayed the three terms. The full results of the analysis are tabulated in Table 3.1.1; these results are examined in the next chapter. The rate diagrams, along with the calculated curves, are presented in Appendix 5.

TABLE 3.1.1 THE ACTIVATION PARAMETERS

	SPECIMEN	$_1V^1$ (b^3)	$\delta\rho_{t1}A^1$ (kg/mm^{2}min)	$_2V^2$ (b^3)	$\delta\rho_{t2}A^2$ (kg/mm^{2}min)	$^1V_2$ (b^3)	$\delta\rho_t{}^1A_2$ (kg/mm^{2}min)	T (^{0}K)
1	C	15	9.91E-5	37	6.74E-6	---	--------	300
2	D	13	1.61E-4	48	7.40E-5	---	--------	300
3	6	14	5.37E-4	--	--------	---	--------	300
4	8	15	4.49E-4	--	--------	---	--------	300
5	9	14	3.70E-4	36	8.46E-5	---	--------	301
6	15	11	3.06E-3	29	3.81E-4	---	--------	300
7	17	12	1.68E-3	--	--------	---	--------	300
8	18	12	1.07E-3	47	6.48E-5	---	--------	300
9	22	13	9.10E-4	44	2.46E-5	---	--------	300
10	23	12	1.03E-3	27	8.07E-5	---	--------	300
11	25	13	8.06E-4	32	3.74E-5	252	4.67E-2	300
12	27	14	1.98E-3	37	4.47E-4	---	--------	300
13	28	13	3.16E-3	37	1.06E-3	---	--------	300
14	29	13	1.57E-3	30	1.29E-4	---	--------	300
15	30	13	2.20E-4	42	1.18E-5	---	--------	308
16	34	13	2.21E-5	--	--------	---	--------	280
17	36	13	2.35E-4	--	--------	---	--------	280
18	37	14	8.60E-3	54	2.75E-4	---	--------	344
19	38	13	3.21E-5	--	--------	---	--------	258
20	39	12	3.24E-3	44	5.35E-5	---	--------	327
21	40	13	2.24E-3	47	6.19E-5	123	3.36E-2	330
22	41	12	6.50E-3	31	2.26E-4	57	1.08E-1	338
23	42	12	3.09E-3	24	4.53E-4	27	8.95E-2	329
24	43	13	5.76E-4	36	5.18E-5	53	4.39E-3	317
25	44	13	6.83E-3	33	4.12E-4	53	1.14E-1	329

3.2 AN EMPIRICAL REPRESENTATION: THE POWER FUNCTION RELATION

Superplastic materials are usually examined by performing creep tests or constant strain rate experiments. The results of these investigations are represented as some form of the empirical equation

$$\dot{\varepsilon} = K\sigma^n$$

where σ is the steady state flow stress and $\dot{\varepsilon}$ the strain rate; K and n are parameters that depend on material and testing conditions; the values are then plotted as log $\dot{\varepsilon}$ versus log σ. This plot is often sigmoidal, defining three zones where n is considered to be constant. Superplastic behavior occurs in the region of minimum n where values from 1.25 to 2.00 are typically reported at superplastic conditions.

The results of the experiments were plotted in the log (-R) versus log τ_a coordinate system as shown in Figure 3.2.1. The applied stress was used instead of the effective stress for better comparison with the literature. Lines were fitted in the minimum slope region of these plots; these values are listed in Table 3.2.1. The results are discussed in the next chapter.

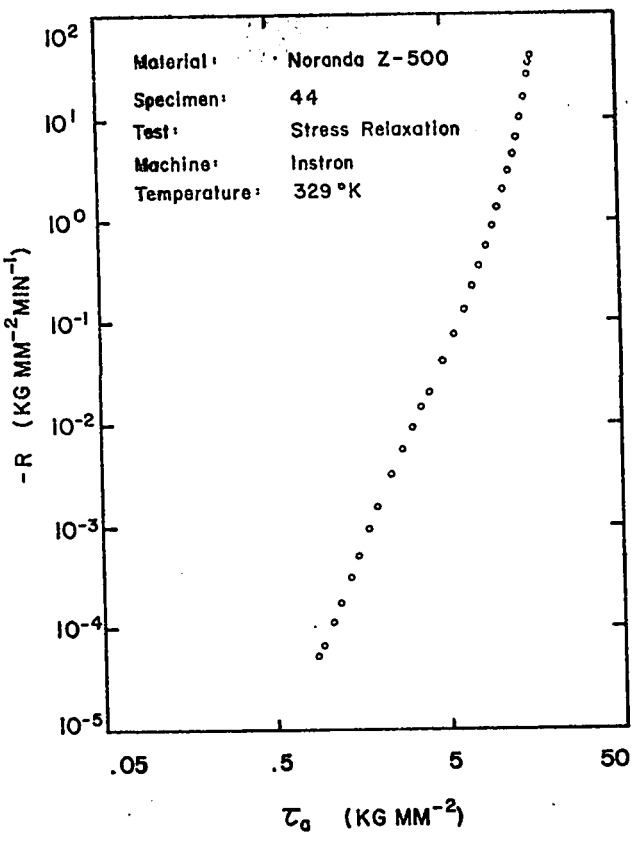

Figure 3.2.1 The determination of the stress exponent.

TABLE 3.2.1 THE STRESS EXPONENT

	SPECIMEN	n		SPECIMEN	n
1	C	6.7	14	29	2.1
2	D	3.6	15	30	3.2
3	6	---	16	34	4.8
4	8	---	17	36	5.5
5	9	4.0	18	37	2.8
6	15	3.8	19	38	9.3
7	17	4.5	20	39	3.6
8	18	3.6	21	40	3.7
9	22	4.7	22	41	3.5
10	23	2.0	23	42	3.9
11	25	3.2	24	43	4.2
12	27	4.1	25	44	3.7
13	28	3.5			

3.3 THE ACTIVATION ENERGIES

The activation volume is a very important indicator of the nature of the rate controlling processes of plastic flow; an equally significant quantity is the height of the energy barrier, the activation energy. Theoretically rigorous evaluations of these parameters have not yet been done, though some approximate methods have been used in some instances. Experimental data is usually compared to these rough values and conclusions are then put forward as to the nature of the deformation controlling mechanisms.

In the absence of stress, the expression describing the rate of a simple process where activation proceeds in one direction can be written as

$$\text{Rate} = \delta\rho_t A \exp\left(-\frac{\Delta G^{\ddagger}}{kT}\right) \qquad (3.3.1)$$

In the above expression, the temperature dependence of the preexponential factor is neglected since that of the exponential term is much stronger. From the above equation we obtain

$$K \left.\frac{\partial \ln R}{\partial \ln(1/T)}\right|_{\tau_{eff}=0} = -\Delta G^{\ddagger} \qquad (3.3.2)$$

The activation energies are then obtained from a plot of the logarithm of the intercept $\delta\rho_t A$ versus the reciprocal of temperature. Such a figure is called the Arrhenius plot and if the mechanism is temperature independent, the behavior will be that of a straight line of negative slope.

Before plotting such diagrams, the effect of the different testing procedures must be considered. The total strain rate, $\dot{\varepsilon}_t$, can be described as

$$\dot{\varepsilon}_t = \dot{\varepsilon}_p + \dot{\varepsilon}_e \tag{3.3.3}$$

where $\dot{\varepsilon}_p$ is the plastic strain rate and $\dot{\varepsilon}_e$ is the elastic component of the rate, expressed as

$$\dot{\varepsilon}_e = \dot{\sigma}/E \tag{3.3.4}$$

where E is the elastic modulus. In an ideal stress relaxation experiment, the total strain change is zero; then

$$\dot{\varepsilon}_p = -\dot{\varepsilon}_e \quad \text{or} \quad \dot{\varepsilon}_p = -\dot{\sigma}/E \tag{3.3.5}$$

In real tests, this condition is not satisfied; the sum of the machine and specimen deflections is zero, or

$$\dot{\varepsilon}_t + \dot{\varepsilon}_m = 0 \tag{3.3.6}$$

where the subscript m means machine. If the machine deflection is elastic, then

$$\dot{\varepsilon}_t + \dot{\sigma}/K = 0 \tag{3.3.7}$$

where K is the machine stiffness. From Eq. (3.3.3) and (3.3.5) we find

$$\dot{\varepsilon}_p + \dot{\varepsilon}_e + \dot{\sigma}/K = 0$$

$$\text{or} \quad \dot{\varepsilon}_p + \dot{\sigma}(1/E + 1/K) = 0$$

$$\text{and} \quad \dot{\varepsilon}_p = -\dot{\sigma}(1/E + 1/K) = -\dot{\sigma}/E' \tag{3.3.8}$$

where E' is called the combined elastic modulus, a function of both the machine and specimen.

In the experiments performed without the computer control, the total

strain ε_t was measured. From Eq. (3.3.3), (3.3.5) and (3.3.8)

$$\dot{\varepsilon}_t = \dot{\sigma}(1/E - 1/E') \quad \text{or} \quad 1/E' = 1/E - \dot{\varepsilon}_t/\dot{\sigma} \qquad (3.3.9)$$

The last equation gives the necessary relationship between the different testing procedures. The combined elastic modulus was obtained by averaging $\dot{\varepsilon}_t/\dot{\sigma}$ for the experiments where the strain was measured; when the control was used, the effective modulus was considered to be that of the material; these values are listed in Table 3.3.1.

TABLE 3.3.1 THE COMBINED ELASTIC MODULI

Machine	E' (kg/mm^2)
Hounsfield with control	8400
Hounsfield without control	1600
Instron	3800

The intercepts of Table 3.1.1 were then reevaluated to represent the strain rate when the effective stress is zero and are tabulated in Table 3.3.2. An averaging technique was used for the controlled experiments; the value in the table is the arithmetic mean of the logarithm of the intercepts. A discussion of this is included in the next chapter.

The Arrhenius plots were then drawn and the slopes evaluated (Figure 3.3.1). The activation energies were found to be 14.1 kcal/mole for the first term, 11.1 kcal/mole for the second and 12.6 kcal/mole for the third.

TABLE 3.3.2 THE DETERMINATION OF THE ACTIVATION ENERGIES

SPECIMEN	1/T (10^3 $^0K^{-1}$)	$\delta\rho_{t1}A^1/E'$ (min^{-1})	$\delta\rho_{t2}A^2/E'$ (min^{-1})	$\delta\rho_{t}{}^{1}A_2/E'$ (min^{-1})
C	3.33	6.19E-8	4.21E-9	-------
D	3.33	1.00E-7	4.63E-8	-------
9	3.32	9.74E-8	2.23E-8	-------
30	3.25	1.38E-7	7.38E-9	-------
34	3.52	1.38E-8	-------	-------
36	3.57	6.17E-8	-------	-------
37	2.91	5.37E-6	1.72E-7	-------
38	3.88	8.45E-9	-------	-------
39	3.06	2.03E-6	3.34E-8	-------
40	3.03	1.40E-6	3.87E-8	2.10E-5
41	2.97	1.71E-6	5.93E-8	2.85E-5
42	3.04	1.93E-6	2.83E-7	5.59E-5
43	3.15	3.60E-7	3.24E-8	2.74E-6
44	3.04	1.80E-6	1.08E-7	3.00E-5
$\overline{NC}$	3.33	1.47E-7	1.61E-8	5.55E-6

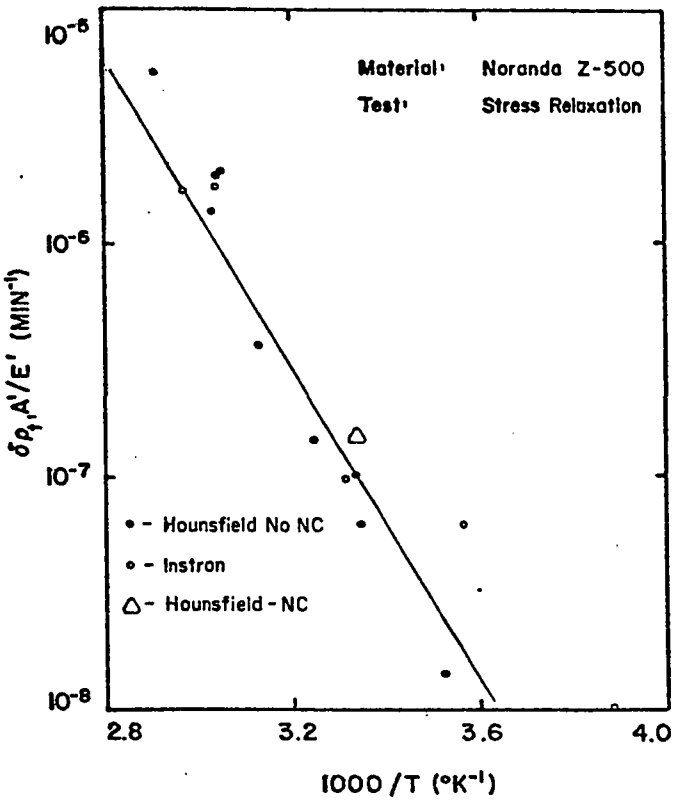

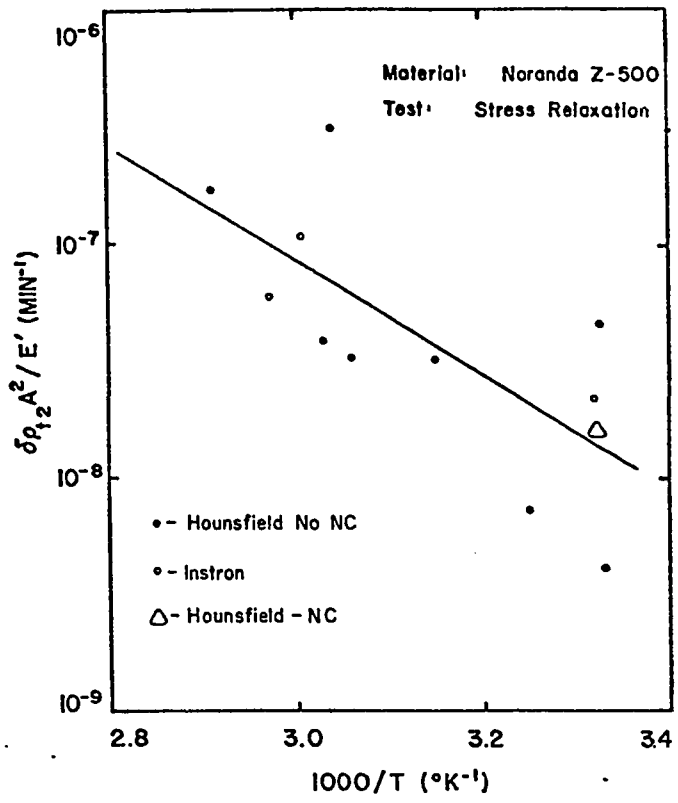

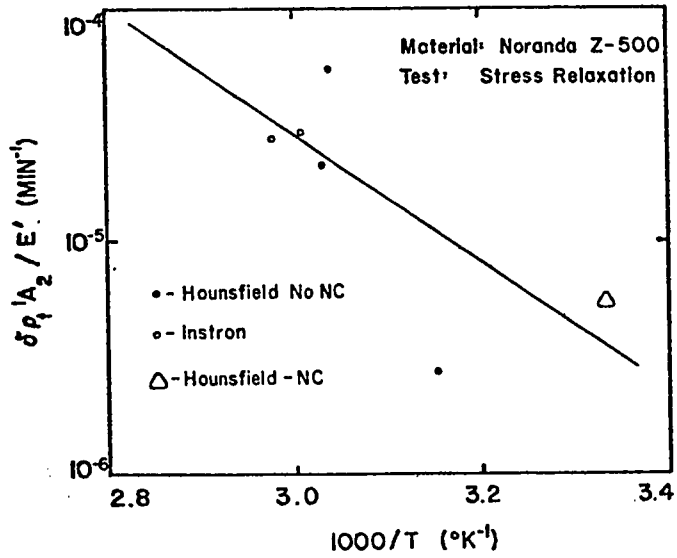

Figure 3.3.1 The Arrhenius plots.

(The letters NC mean 'with Numerical Control').

CHAPTER 4

DISCUSSION AND CONCLUSIONS

4.1 DISCUSSION OF THE EXPERIMENTAL RESULTS

The zinc aluminum alloy studied in this investigation was not tested under superplastic conditions; consequently, direct comparison with existing data is not always possible.

The purpose of this work was twofold; the primary objective was to investigate the deformation behavior of a commercial alloy and as such, the results presented could be used to predict the performance of components manufactured from this material, since the temperature range covered spans that encountered in most commercial applications. As a study of superplastic behavior, this work is no more than a preliminary investigation of the flow properties of the alloy.

The discussion will be centered about this point of view; no conclusions will be drawn as to the commercial applicability of the alloy.

The second objective was to evaluate the performance of the computer control system described in Chapter 2. This will be discussed in the last part of this section.

A. THE SYSTEM OF TWO CONSECUTIVE ENERGY BARRIERS

Mohamed et al. [10,11] have concluded that superplastic flow in a eutectoid Zn-Al alloy was controlled by activation over two consecutive energy barriers; they based their argument on activation energy measurements. These indicated that the activation energy increased with decreasing stress, from which they concluded that deformation resulted from the sequential operation of two different processes. Even though the trend of their experimental data is in agreement with this model, their argument would also be valid for a system where activation proceeds in the backward direction over a single energy barrier or for some system of parallel energy barriers.

Hay and Pascoe [12] have analysed the kinetics of deformation of a superplastic Pb - 38.1% Sn alloy at room temperature with empirical relationships; they concluded that deformation at low stresses was the result of the interdependent action of two mechanisms, or a system of two consecutive barriers. They also suggested that the behavior at high stresses could be due to a third, parallel mechanism.

Zehr and Backofen [13] investigated the deformation behavior of four superplastic lead-tin alloys at temperatures varying from 25 ^{0}C to 170 ^{0}C. They reported that the observed stress - strain rate relationships could be described by a combination of two parallel mechanisms acting in series with a third. However, this formulation could not be fitted to their data;

instead, a system of two consecutive barriers, acting in parallel with a third, was found to match their results. Further analysis of their data showed that the parallel mechanism had very little influence on the deformation rates.

In a study of the flow characteristics of the Zn - 22% Al eutectoid and the Pb - 62% Sn eutectic, Mohamed and Langdon [14] suggested that two consecutive mechanisms governed the superplastic behavior at high stresses, while a third, parallel mechanism was rate-controlling at low stresses.

Prematta, Venkatesan and Pense [15] have reported that the deformation kinetics of a superplastic tin-zinc eutectic alloy could be described by forward and backward activation over a single energy barrier.

Other works on superplasticity normally do not report on the kinetics of the processes; the data is generally represented by some form of the empirical equation $\dot{\varepsilon} = K\sigma^n$, where K and n are parameters which are functions of the grain size, diffusion coefficient, temperature, material properties and stress; typically, K and n take three values, with each of them describing the behavior in three separate ranges of applied or effective stress.

The results of a study of the zinc-aluminum eutectoid by Ball and Hutchison [16] were analysed with the equations of deformation kinetics and the behavior matched that of the model proposed in this work.

From these considerations and from the good agreement of the different experimental techniques used in this project, it is concluded that the model of two consecutive mechanisms controlling the deformation of at least certain superplastic alloys at near room temperatures fits the observed data.

B. *THE ACTIVATION VOLUMES*

Faucher and Krausz [17] have shown that the stress at which the second barrier becomes dominant can be expressed as

$$\tau_1 = \frac{{}_1\Delta G^{1\ddagger} - {}_2\Delta G^{2\ddagger}}{{}_1V^1 - {}_2V^2} \qquad (4.1.1)$$

This value was found to be approximately 5 kg/mm^2. The activation energies and volumes as expressed above are usually considered to be independent of temperature; consequently, as the temperature is increased and the yield stress drops, there will be a temperature T_1 at which the stress will never exceed τ_1. It is then expected that, at temperatures higher than T_1, the first barrier will not be rate-controlling.

Chaudari [18] reported an increase in the activation energy from an Arrhenius plot at approximately 190 ^{0}C for the zinc-aluminum eutectoid. The conclusion to be drawn from this argument is that the first term to become evident in the deformation of the alloy is ${}_1k^1$ at temperatures

lower than 190 ^{0}C and $_2k^2$ at higher temperatures.

The activation volumes for stresses higher than τ_1 were found to be 13 ± 1 b^3, while the corresponding value obtained from Ball and Hutchison's data at 150 ^{0}C is 14 b^3. The analysis of Ball and Hutchison's data further yielded values for $_2V^2$ of 28 b^3 at 150 ^{0}C and 250 ^{0}C while those reported in this investigation are 38 ± 14 b^3 for temperatures ranging from 30 ^{0}C to 74 ^{0}C.

At lower stresses, values of $^1V_2$ ranging from 100 to 150 b^3 are shown by Lee and Niessen [19] for a near-eutectoid zinc-aluminum alloy deformed at 204 ^{0}C, while Ball and Hutchison's results indicate 101 b^3 at 250 ^{0}C. The corresponding values tabulated in this report vary from 27 to 252 b^3.

Theoretical evaluations give only the order of magnitude of the activation parameters; this reflects the uncertainties encountered when dealing with deformation processes. As such, there is very good agreement between the results of this investigation and those reported by others; the increasing scatter in the activation volumes as the stress decreases is expected since the experimental error and decreasing relative sensitivity of the instrumentation at the lower stress rates is naturally affecting the experimental values.

C. THE STRESS EXPONENT

The value of the stress exponent or its inverse, the strain rate sensitivity, is usually used as an indicator of superplasticity. When $n = 1$, Equation (3.2.1) reduces to that describing Newtonian viscous flow; consequently, the smaller the value of n, the more enhanced the superplastic properties. Materials with a stress exponent smaller than three are usually superplastic.

The stress exponent is a function of temperature, strain rate and grain size as follows: [1] n will decrease with increasing temperature and decreasing grain size and it will go through a minimum with increasing strain rate, defining the range of strain rates at which superplastic behavior occurs.

No data was found to compare with the stress exponents obtained in this analysis; however, the low values of n at the temperatures tested do point to the superplastic properties of the material.

D. THE ACTIVATION ENERGIES

There is considerable discrepancy in the published data for the activation energies of superplastic flow in the zinc-aluminum eutectoid (References 11, 16, 20, 21, 22, 23); at high strain rates, values between 23 and 29 kcal/mole are reported. At intermediate strain rates, these range from 18 to 39 kcal/mole, while at low rates the reported activation energies vary from 15 to 29 kcal/mole. The corresponding values reported in this investigation are 14.1, 11.1 and 12.6 kcal/mole.

The determination of the activation energies is the aspect of this analysis that is most subject to error; the values listed in Table 3.3.2 are dependent on accurate measurements of the internal stress and combined elastic moduli.

The internal stress was assumed to remain constant during relaxation; Lee and Niessen [19] studied its variation with strain rate in a similar alloy and reported a change of approximately 0.1 kg/mm^2 over four orders of magnitude of strain rate. This variation is obviously not too significant and would not explain the scatter in the Arrhenius plots.

In a similar study, Mohamed and Langdon [20] discussed the determination of the activation energy for superplastic flow; they included in their analysis the temperature dependence of the shear modulus. In view of the small temperature range covered in the present investigation, this

variation was neglected.

Another assumption made in the analysis of the activation energies was that the controlled relaxation experiments were machine-independent, which is not entirely valid. As can be seen from Figure 2.1.1, the controlled, stepwise relaxation will approximate the ideal relaxation procedure only as $\Delta\varepsilon_t$ becomes very small. Since all controlled experiments were performed under similar conditions, this does not explain the wide scatter in the values of the intercepts.

The activation energies obtained from the Arrhenius plots do not fit the model of two consecutive energy barriers. It is obvious from the rate diagrams that $\delta\rho_{t1}A^1$ is larger than $\delta\rho_{t2}A^2$; consequently ${}_1\Delta G^{1\ddagger}$ should be smaller than ${}_2\Delta G^{2\ddagger}$, while the analysis of section 3.3 shows the opposite.

No satisfactory explanation was found that would account for the discrepancies encountered in the determination of the activation energies. It was then concluded that further experiments should be designed to investigate the activation energies for plastic flow in this alloy; these would include a study of the effect of computer control on the rigidity of the testing apparatus.

E. THE DEFORMATION MECHANISMS

Several mechanisms have been proposed to explain superplasticity, but no model accounts for the full behavior of such materials. It is generally recognized that more than one mechanism operate; Ashby and Verall [25] described a model based on grain boundary sliding with diffusional accommodation and, while this model does not predict accurate values for strain rates, it is believed that grain boundary sliding is the dominant mechanism and that the flow is aided by one or two other mechanisms. [1,24]

No conclusion will be drawn as to the nature of the deformation mechanisms with the exception that, for the zinc-aluminum eutectoid, the mechanisms are dependent on each other.

F. COMPUTER CONTROLLED STRESS RELAXATION

The recent appearance on the market of inexpensive mini and micro computers has made possible the introduction of numerical control systems in applications where the cost had previously been prohibitive. The system described in this report was used to control stress relaxation experiments; it could also be used to control creep tests, constant strain rate tests, or any combination of such experiments. The application of a control system can also warrant the use of less expensive testing machines, since the controller can approximate the behavior of more costly machines

such as the Instron. It is also possible to control more than one experiment with one computer, thus further reducing the cost of complex testing systems.

However, as this study showed, the effect of the controls on the behavior of the material should be further studied. It is nevertheless believed that the use of the control system is warranted; the introduction of more sophisticated peripherals such as a more stable amplifier for the extensometer signal would help reduce the control limits ($\Delta\varepsilon_t$), and thus improve the effectiveness of the control.

4.2 CONCLUSIONS

A. The deformation kinetics of a near-eutectoid zinc-aluminum alloy at near-room temperatures can be represented by a system of two consecutive energy barriers. The strain rate is expressed as

$$\dot{\varepsilon} = \frac{\delta\rho_t \frac{kT}{h}}{\exp\left(\frac{{}_1\Delta G^1}{kT}\right) + \exp\left(\frac{{}_2\Delta G^2}{kT}\right) + \exp\left(\frac{{}_1\Delta G^2}{kT}\right)} \qquad (4.2.1)$$

B. It is postulated that the full expression for the strain rate at higher temperatures would include the term describing backward activation over the two barriers as

$$\dot{\varepsilon} = \delta\rho_t \frac{kT}{h} \frac{1 - \exp\left(\frac{{}_1\Delta G_1}{kT}\right)}{\exp\left(\frac{{}_1\Delta G^1}{kT}\right) + \exp\left(\frac{{}_2\Delta G^2}{kT}\right) + \exp\left(\frac{{}_1\Delta G^2}{kT}\right)} \qquad (4.2.2)$$

where the first term in the denominator would not be present at temperatures higher than 190 ^{0}C.

C. The activation volumes were calculated to be 13 ± 1 b^3 for the first term, 38 ± 14 b^3 for the second and varied from 27 b^3 to 252 b^3 for the third.

D. The stress exponent was found to vary from 2.1 to 9.3; these values are sufficiently low to predict superplastic flow at higher temperatures.

E. It was not possible to determine accurate values for the activation energies.

F. The deformation mechanisms are dependent on each other, though it is not possible to identify them without further experiments.

G. Computer controlled experiments are valid; the influence of the control on the results should however be further investigated.

BIBLIOGRAPHY

1. G. J. Davies, J. W. Edington, C. P. Cutler and K. A. Padmanabhan, J. Mat. Sci., 5, (1970), 1091-1102.

2. H. M. Weld, "*Superplasticity*", Information Circular IC235, Dept. of Energy, Mines and Ressources, Mines Branch, Ottawa, Oct. 1969.

3. Noranda Mines Ltd., "*Superplastic Conditioning of Ternary and Quaternary Zinc-Aluminum Alloys*", Canadian Patent No. 940807, Class 148-30, C.R.C.L. 80-51, Issued Jan. 29, 1974.

4. G. Seibel, Formages Traitements Métaux, 32, (Feb. 1972), 17-25.

5. Noranda Mines Ltd.,"*Screw Machining Material and Method of Preparing Same*", Canadian Patent No. 939535, Class 75-77, C.R.C.L. 148-10, Issued Jan. 8, 1974.

6. A. S. Krausz and H. Eyring, "*Deformation Kinetics*", Wiley-Interscience, New York, 1975.

7. A. S. Krausz, W. H. Ginman, G. Toth and J. Jakab, unpublished, 1975.

8. G. B. Gibbs, Phil. Mag., 13, (1966), 317-329.

9. T. O'D. Hanley and A. S. Krausz, J. Appl. Phys., 45, 5, (May 1974), 2013-2015.

10. F. A. Mohamed and T. G. Langdon, Acta Met., 23, (Jan. 1975), 117-124.

11. F. A. Mohamed, S. A. Shei and T. G. Langdon, Acta Met., 23, (Dec. 1975),. 1443-1450.

12. K. A. Hay and R. T. Pascoe, J. Mat. Sci., 9, (1974), 1285-1289.

13. S. W. Zehr and W. A. Backofen, Trans. ASM, 61, (1968), 300-313.

14. F. A. Mohamed and T. G. Langdon, Scr. Metall., 10, (1976), 759-762.

15. R. J. Prematta, P. S. Venkatesan and A. Pense, Metall. Trans. A, 7A, (Aug. 1976), 1235-1236.

16. A. Ball and M. M. Hutchison, Met. Sci. J., 3, (1969), 1-7.

17. B. Faucher and A. S. Krausz, J. Appl. Phys., (submitted).

18. P. Chaudari, Acta Met., 15, (1967), 1777-1786.

19. J. D. Lee and P. Niessen, J. Mat. Sci., 9, (1974), 1467-1477.

20. F. A. Mohamed and T. G. Langdon, Physica Status Solidi (a), 33, (1976), 375-381.

21. K. A. Padmanabhan and G. J. Davies, Physica Status Solidi (a), 18, (1973), 295-302.

22. P. Maulik and K. A. Padmanabhan, J. Mat. Sci., 10, (1975), 1646-1649.

23. H. Naziri, R. Pearce, M. Henderson Brown and K. F. Hale, Acta Met., 23, (1975), 489-496.

24. M. L. Vaidya, K. Linga Murty and J. E. Dorn, Acta Met., 21, (1973), 1615-1623.

25. M. F. Ashby and R. A. Verrall, Acta Met., 21, (Feb. 1973), 149-159.

26. T. A. Alden in "*Treatise on Material Science and Technology*", vol. 6, R. J. Arsenault ed., Academic Press, New York, 1975, 226-266.

27. C. H. Reinsch, Num. Math., 10, (1967), 177-183.

28. T. N. E. Greville in "*Theory and Applications of Spline Functions*", T. N. E. Greville ed., Academic Press, New York, 1969, 1-35.

29. Reference Manual, IMSL Library 1, 5th edition, International Mathematics and Statistical Libraries Inc., Houston, Texas, U.S.A., 1975.

30. "*Operating and Programming the Hewlett Packard 9810A Calculator*", Hewlett Packard Co. Ltd., Manual No. 09810-90000, 1971.

APPENDICES

APPENDIX 1: THE PROPERTIES OF Z-500

Noranda's Z-500 is a zinc base material with an alloying composition of 25 w/o aluminum, 5 w/o copper and 0.05 w/o magnesium; it is marketed as a free cutting alloy and recommended applications include screw machine and hot forged parts. A table of its physical and mechanical properties follows(*). A true stress - true strain curve is shown in Figure A.1.1.

TABLE A.1.1 THE PROPERTIES OF Z-500

PHYSICAL PROPERTIES	UNITS	
Melting Point (Liquidus)	^0F	891 (477 ^0C)
Melting Point (Solidus)	^0F	752 (400 ^0C)
Density	lb/in^3	0.184 (5.09 g/cc)
Specific Gravity		5.09
Electrical Resistivity	ohms (cir.mi./ft)	30.7
Electrical Conductivity	% IACS	32
Thermal Capacity	$BTU/lb/^0F$	0.125
Modulus of Elasticity	psi x 10^6	12 (8400 kg/mm^2)
Lattice Parameter	A^0	2.7
MECHANICAL PROPERTIES		
Tensile Strength	psi	66,000 (46.4 kg/mm^2)
Yield Strength, 0.2% offset	psi	54,000 (38.0 kg/mm^2)
Reduction of Area	%	38
Elongation in 2"	%	24
Hardness	Rockwell	B77

* - adapted from an information circular issued by Noranda.

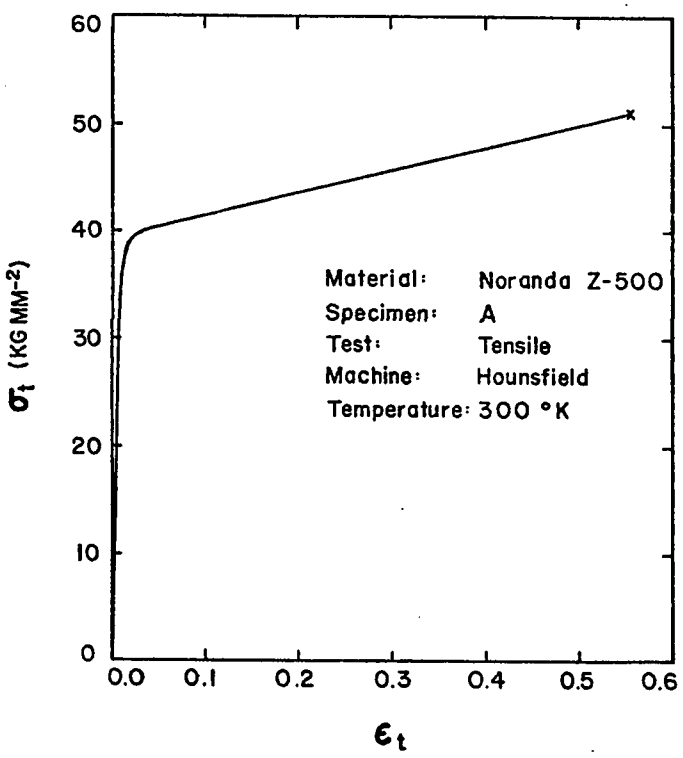

Figure A.1.1 A true stress - true strain curve measured at an initial strain rate of 0.008/min.

APPENDIX 2: THE DERIVATION OF EQUATION (1.2.15)

The following substitutions were made in Eq. (1.2.15):

$$\frac{{}^{1}k_{2}\,{}^{2}k_{1}}{{}_{1}k^{1}\,{}_{2}k^{2}} = \exp\left(\frac{{}^{1}\Delta G_{1}}{kT}\right), \tag{A.2.1}$$

$$\frac{{}^{1}k_{2}}{{}_{1}k^{1}\,{}_{2}k^{2}} = \exp\left(\frac{{}^{1}\Delta G^{2}}{kT}\right), \tag{A.2.2}$$

and

$$\frac{{}^{2}k_{1}}{{}_{1}k^{1}\,{}_{2}k^{2}} = \exp\left(\frac{{}^{2}\Delta G^{1}}{kT}\right) \tag{A.2.3}$$

where each rate constant is of the form

$$k = \frac{kT}{h}\exp\left(-\frac{\Delta G}{kT}\right). \tag{A.2.4}$$

Then,

$$\frac{{}^{1}k_{2}\,{}^{2}k_{1}}{{}_{1}k^{1}\,{}_{2}k^{2}} = \frac{\exp\left(-\frac{{}^{1}\Delta G_{2}}{kT}\right)\exp\left(-\frac{{}^{2}\Delta G_{1}}{kT}\right)}{\exp\left(-\frac{{}^{1}\Delta G^{1}}{kT}\right)\exp\left(-\frac{{}^{2}\Delta G^{2}}{kT}\right)} = \exp\left(\frac{{}^{1}\Delta G^{1} - {}^{1}\Delta G_{2} + {}^{2}\Delta G^{2} - {}^{2}\Delta G_{1}}{kT}\right)$$

And, from Figure 1.2.5 and as shown in Figure A.2.1

$$\frac{{}^{1}k_{2}\,{}^{2}k_{1}}{{}_{1}k^{1}\,{}_{2}k^{2}} = \exp\left(\frac{{}^{1}\Delta G_{1}}{kT}\right). \tag{A.2.5}$$

Similarly,

$$\frac{{}^{1}k_{2}}{{}_{1}k^{1}{}_{2}k^{2}} = \frac{h}{kT} \exp\left(\frac{-{}^{1}\Delta G_{2} + {}_{1}\Delta G^{1} + {}_{2}\Delta G^{2}}{kT}\right) = \frac{h}{kT} \exp\left(\frac{{}_{1}\Delta G^{2}}{kT}\right) \qquad \text{(A.2.6)}$$

And

$$\frac{{}^{2}k_{1}}{{}_{1}k^{1}{}_{2}k^{2}} = \frac{h}{kT} \exp\left(\frac{-{}^{2}\Delta G_{1} + {}_{1}\Delta G^{1} + {}_{2}\Delta G^{2}}{kT}\right) = \frac{h}{kT} \exp\left(\frac{{}_{2}\Delta G^{1}}{kT}\right). \qquad \text{(A.2.7)}$$

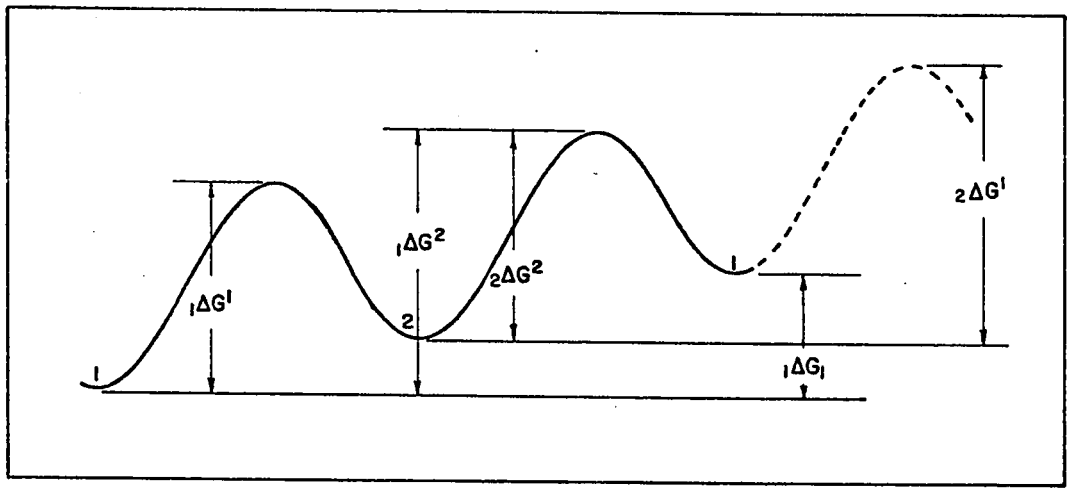

Figure A.2.1 The apparent free energies associated with Eq. (1.2.15).

APPENDIX 3: NUMERICAL ANALYSIS

A.3.1 NUMERICAL DIFFERENTIATION BY SMOOTH SPLINE FUNCTIONS

A common method in fitting curves to experimental data uses least-square polynomials; however, the high order polynomials needed to represent complex curves often yield erratic values for derivatives. Spline functions are used in order to obtain interpolating polynomials through the experimental data. A smooth cubic spline will fit polynomials between all experimental points such that the polynomials and their first and second derivatives will be continuous everywhere and that the polynomials will pass within a certain defined vicinity of the experimental points.

The theory of cubic splines will not be included here; the interested reader is recommended to references (27) and (28) for more information.

A colleague, Mr. B. Faucher, had previously written an APL program to obtain the stress rates from experimental stress and time data using this technique. This program was tested against the results of graphical differentiation and, as mentioned in section 3.1, was found satisfactory; the method was then applied for all experiments.

A.3.2 NON-LINEAR LEAST-SQUARE CURVE FITTING

The step-by-step method used in the evaluation of the activation parameters requires prior knowledge of any term acting before the one under analysis; in other words, the description of the second term will depend on the numerical values assigned to the first and similarly, that of the third depends on the values describing the first and second.

Independent least-square evaluations of the linear portions of the experimental plots such as those shown in Figures 3.1.2, 3.1.4 and 3.1.5 were found to be too subjective and prone to error. A FORTRAN program was then written to fit a least-square curve of the form described by the equations of deformation kinetics. The basic subroutine of this program includes an algorithm whose function is to estimate the activation parameters such that the residual sum of squares is minimized, in the usual least-square sense; this subroutine is called ZXSSQ and is part of a commercial software package called IMSL [29].

A drawback of this method is that it requires relatively accurate initial guesses for the values of the parameters (typically within 10% of the optimal values); however, since this involved some graphical evaluation, it provided an opportunity to reject any data that was obviously in error. This method was applied for all experimental evaluation; the solid lines in the plots of section 3.1 and Appendix 5 were obtained from this analysis.

APPENDIX 4: COMPUTER CONTROLLED STRESS RELAXATION

The purpose of the control system was to constantly monitor the experiment and to take appropriate action when required. This appendix describes the hardware and the software of this system.

A.4.1 THE CONTROL SYSTEM

Figure A.4.1 shows a photograph of the control system, along with a system flowchart. The main components of this system and their functions are:

A. Hewlett Packard 9810A Programmable Calculator: the basis of the system; the calculator controls all aspects of the experiment through a suitable program.

B. Code Converter (Hewlett Packard 2575A Coupler/Controller): serves as a translator between the calculator and other components.

C. Hewlett Packard 3480B Digital Voltmeter: provides analog to digital conversion of the extensometer signal; it also serves as a system performance monitor through its digital display.

D. Controller: accepts the data from the code converter and sequentially feeds it to the power amplifier.

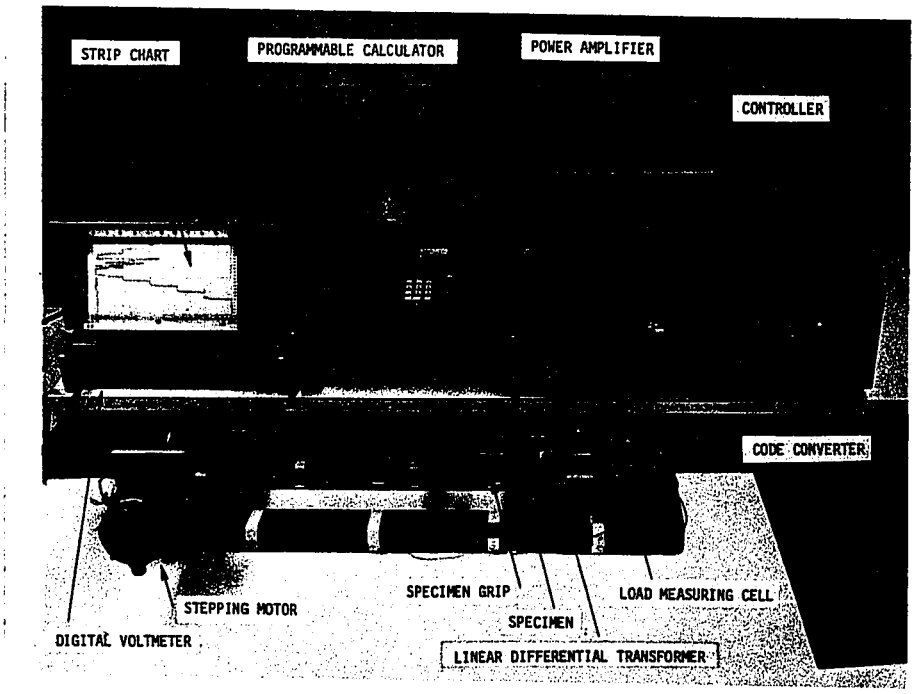

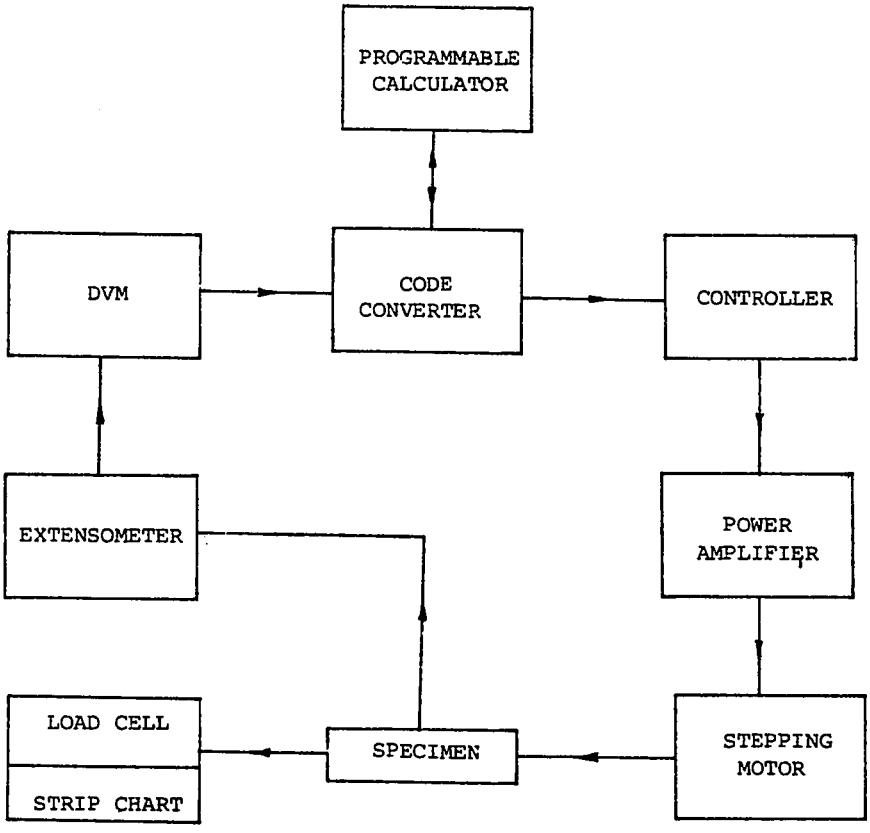

Figure A.4.1 The control system.

E. Power Amplifier: translates the digital information from the controller to power pulses in order to energize the stepping motor.

F. Stepping Motor (American Superior Electric Slo-Syn Model M112): drives the tensometer.

A.4.2 THE CONTROL ALGORITHM

The control algorithm had to be written in such a way as to maximize the feedback frequency; as such the algorithm had to be kept as simple as possible. Essentially, the program would request a reading of length, check if that reading was within some prescribed limits, ($\Delta\varepsilon_t$ in Figure 2.1.1 or $\pm\Delta L_t$ in the program listing) and would, if required, move the tensometer crosshead the proper distance to bring the specimen's length back within the limits. When five readings had been taken and no corrections had been made, the control would branch to a subroutine which would fit a least-square line through the five readings and predict the next; this predicted value would then be checked against the limits. Following are a flowchart and a listing of the program; the listing is written in the language of the calculator, which is explained in reference (30).

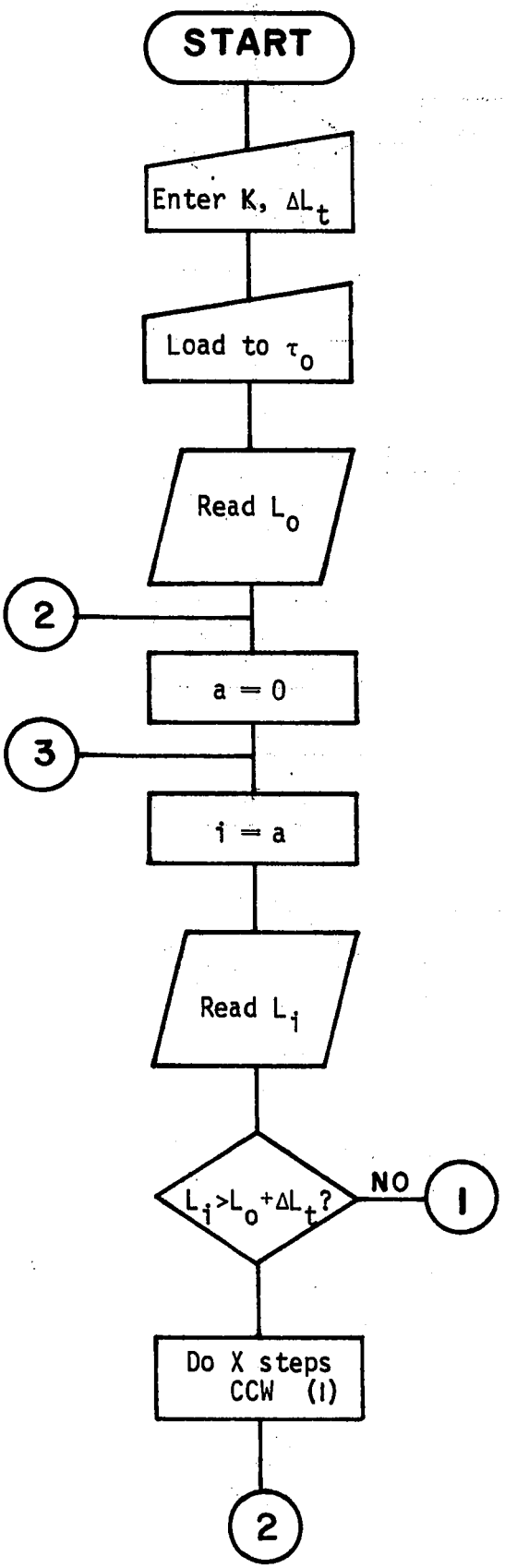

Figure A.4.2 The control program flowchart.

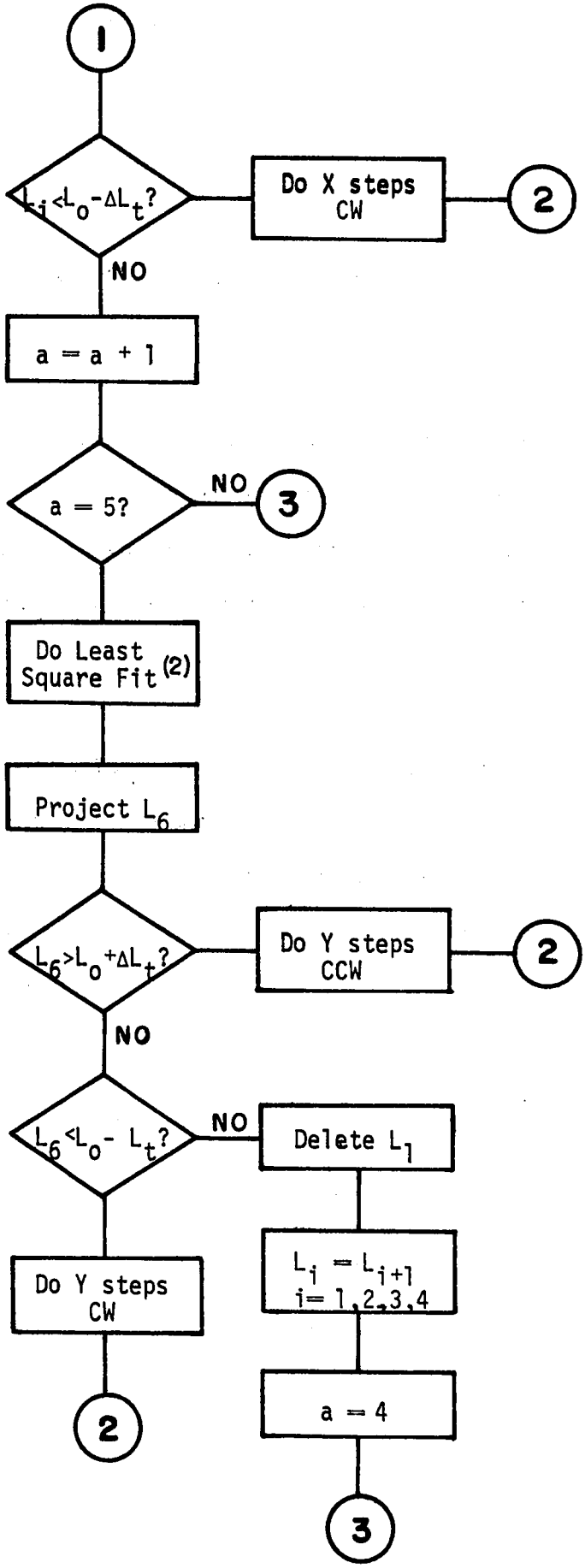
1
$L_i < L_o - \Delta L_t$?
Do X steps CW
2
NO
a = a + 1
a = 5?
NO
3
Do Least Square Fit (2)
Project L_6
$L_6 > L_o + \Delta L_t$?
Do Y steps CCW
2
NO
$L_6 < L_o - L_t$?
NO
Delete L_1
$L_i = L_{i+1}$ i= 1,2,3,4
a = 4
3
Do Y steps CW
2

NOTES:

1. The number of steps (X or Y) is proportional to the error and is calculated as follows:

$$X = K\ |\Delta L| \qquad (A.4.1)$$

where K is a proportionality constant, dependent on the machine and extensometer (K = 15,000 steps/volt for the Instron G51-12 extensometer mounted on the Hounsfield); ΔL is the deviation from the initial length, measured in volts. The quantity X (or Y) must then be properly formatted for the controller.

2. The least-square fit follows from the usual first degree polynomial formulas; the abscissae are dummy variables, x_i, which are assigned the values -2, -1, 0, 1, 2; the ordinates are the length readings L_i, i = 1, 2, 3, 4, 5. The expressions for the slope (b_1) and the intercept (b_0) are then

$$b_1 = \frac{n\sum_{i=1}^{n} x_i L_i - \left(\sum_i x_i\right)\left(\sum_i L_i\right)}{n\sum_i x_i^2 - \left(\sum_i x_i\right)^2} = \cdots = \frac{2L_5 + L_4 - L_2 - 2L_1}{10} \qquad (A.4.2)$$

and

$$b_0 = \frac{\sum_i y_i - b_1 \sum_i x_i}{n} = \cdots = \frac{\sum_{i=1}^{5} L_i}{5}\ . \qquad (A.4.3)$$

H·P PROGRAM FORM

TITLE STRESS RELAXATION CONTROL PROGRAM PAGE 1 OF 7

PROGRAMMER Clément Laforce

STEP	KEY	X	Y	Z	a	b	COMMENTS
ØØØØ	GTO	Ø	Ø	Ø	Ø	Ø	
-	S/R						Take initial length
-	1						reading, L_o.
-	2						
-	2						
ØØØ5	UP	L_o	L_o				
-	UP			L_o			Calculate limits
-	PNT						$L_o \pm \Delta L_t$ and store.
-	PNT						
-	XFR						
ØØ1Ø	-						
-	Ø	$L_o - \Delta L_t$					
-	XTO						
-	7						
-	DN	L_o					
ØØ15	XFR						
-	+						
-	Ø	$L_o + \Delta L_t$					
-	XTO						
-	6						
ØØ2Ø	CLR	Ø	Ø	Ø	$i = Ø$	Ø	Initialize counters.
-	GTO						
-	S/R						
-	1						Take length reading, L_i.
-	2						
ØØ25	2						
-	XTO	L_i					
-	IND						
-	a						
-	UP		L_i				
ØØ3Ø	XFR						
-	6						
-	X<Y	$L_o + \Delta L$					Compare new reading
-	SFL						to upper limit.
-	GTO						
ØØ35	S/R						YES--Correction needed.
-	1						
-	4						
-	1						
-	IFG						

MAIN CONTROL ALGORITHM

REGISTERS

ØØØ	ØØ1	ØØ2	ØØ3	ØØ4	ØØ5	ØØ6	ØØ7	ØØ8	ØØ9
ΔL_t, L_1	L_2	L_3	L_4	L_5	---	$L_0 + \Delta L$	$L_o - \Delta L$	K	---

NOTE: Registers ØØØ and ØØ8 must be loaded prior to execution.

H·P PROGRAM FORM

TITLE STRESS RELAXATION CONTROL PROGRAM PAGE 2 OF 7

PROGRAMMER Clément Laforce

STEP	KEY	X	Y	Z	a	b	COMMENTS
0040	0						Correction done, restart.
-	0						
-	2						
-	0						
-	XFR						
0045	7	$L_o - \Delta L$	L_i				
-	X>Y						Compare to lower limit.
-	SFL						
-	GTO						
-	S/R						
0050	1						YES--Correction needed.
-	5						
-	4						
-	IFG						
-	0						
0055	0						Correction done, restart.
-	2						
-	0						
-	1	1					
-	XTO						
0060	+						No correction needed,
-	a				i= i+1		increment counters.
-	UP		1				
-	XFR						Check if control comes from
-	9						least-square or not
0065	X=Y	0 or 1					(if yes, reg.9 contains 1).
-	0						
-	0						YES--Control comes from
-	8						Least-Square.
-	8						
0070	a	i					NO.
-	UP		i				
-	5						
-	X>Y						
-	0						Check if 5 readings
0075	0						were taken; if yes, go
-	2						to least-square; if no,
-	1						take another reading.
-	GTO						
-	S/R						

REGISTERS

000	001	002	003	004	005	006	007	008	009
L_1	L_2	L_3	L_4	L_5	---	$L_o+\Delta L$	$L_o-\Delta L$	K	0 or 1

H·P PROGRAM FORM

TITLE STRESS RELAXATION CONTROL PROGRAM PAGE 3 OF 7

PROGRAMMER Clément Laforce

STEP	KEY	X	Y	Z	a	b	COMMENTS
ØØ8Ø	1						
-	9						
-	4						
-	GTO	L_6					Least-square done, check
-	Ø						if projection within
ØØ85	Ø						limits.
-	3						
-	Ø						
-	CLR	Ø	Ø	Ø	Ø	Ø	
-	XTO						Extrapolation within
ØØ9Ø	9						limits, pause.
-	PSE						
-	PSE						
-	PSE						
-	1	1					
ØØ95	XTO						Delete first reading and
-	+						set $L_i = L_{i+1}$
-	a				i= i+1	j= j-1	$i = 1,2,3,4.$
-	XFR						
-	IND						
ØIØØ	a	L_i					
-	XTO						
-	IND						
-	b						
-	1	1					
Ø1Ø5	XTO						
-	+						
-	b					j= j+1	
-	a	i					
-	UP		i				
Ø11Ø	5	5					
-	X>Y						
-	Ø						
-	Ø						
-	9						
Ø115	4						
-	4	4					
-	XTO						Resetting done, continue
-	a				i = 4		with L_5.
-	GTO						

REGISTERS

ØØØ	ØØ1	ØØ2	ØØ3	ØØ4	ØØ5	ØØ6	ØØ7	ØØ8	ØØ9
L_1	L_2	L_3	L_4	L_5	---	$L_0 + \Delta L$	$L_0 - \Delta L$	K	Ø or 1

H·P PROGRAM FORM

TITLE STRESS RELAXATION CONTROL PROGRAM PAGE 4 OF 7

PROGRAMMER Clément Laforce

STEP	KEY	X	Y	Z	a	b	COMMENTS
Ø12Ø	2						
-	1						
-	FMT						
-	4						
-	4						
Ø125	FMT						READ subroutine.
-	RUP						
-	3						
-	I						
-	RUP						
Ø13Ø	1						
-	E						
-	RUP						
-	1						
-	0						
Ø135	FMT						
-	FMT						
-	3						
-	4						
-	.	L_i					
Ø14Ø	S/R						
-	UP	$L_o + \Delta L$	$L_o + \Delta L$	L_i			
-	2	2					Direction code Ø2 and
-	2	22					feed rate 2Ø ipm stored
-	EEX						in register b.
Ø145	CHS						
-	7	22E-7					
-	XTO						
-	b						
-	GTO						
Ø15Ø	Ø						
-	1						
-	6						
-	2						
-	UP	$L_o - \Delta L$	$L_o - \Delta L$	L_i			
Ø155	1	1					Direction code Ø1 and
-	2	12					feed rate 2Ø ipm stored
-	EEX						in register b.
-	CHS						
-	7						

DIRECTION AND FEED CODES

DATA INPUT

DATA FORMATTING AND OUTPUT

REGISTERS

ØØØ	ØØ1	ØØ2	ØØ3	ØØ4	ØØ5	ØØ6	ØØ7	ØØ8	ØØ9
L_1	L_2	L_3	L_4	L_5	---	$L_o + \Delta L$	$L_o - \Delta L$	K	Ø or 1

H·P PROGRAM FORM

TITLE STRESS RELAXATION CONTROL PROGRAM PAGE 5 OF 7

PROGRAMMER Clément Laforce

STEP	KEY	X	Y	Z	a	b	COMMENTS
Ø16Ø	XTO						
-	b						
-	DN	$L_o \pm \Delta L$	L_i	L_i			
-	-		ΔL				
-	G		$\lvert\Delta L\rvert$				
Ø165	XFR						
-	8						
-	X	K	$K\lvert\Delta L\rvert$				Round-off correction and
-	Ø						add codes.
-	K						
Ø17Ø	9	Round-off					
-	XEY	$K\lvert\Delta L\rvert$	Round-off				
-	1	1	(R)				
-	EEX						
-	4	1Ø,ØØØ					
Ø175	DIV		R/1ØØØØ				
-	YE						
-	+						
-	b		Correction				
-	DN	Correction					
Ø18Ø	FMT						
-	4						Output command.
-	4						
-	FMT						
-	RUP						
Ø185	3						
-	I						
-	RUP						
-	Ø						
-	I						
Ø19Ø	PNT						
-	LBL						
-	FMT						
-	S/R						
-	CLR	Ø	Ø	Ø	Ø	Ø	
Ø195	YE						
-	+						LEAST SQUARE FIT THROUGH
-	IND						FIVE READINGS.
-	a		ΣL_i				
-	1	1					

REGISTERS

ØØØ	ØØ1	ØØ2	ØØ3	ØØ4	ØØ5	ØØ6	ØØ7	ØØ8	ØØ9
L_1	L_2	L_3	L_4	L_5	---	$L_o + \Delta L$	$L_o - \Delta L$	K	Ø or 1

H·P PROGRAM FORM

TITLE STRESS RELAXATION CONTROL PROGRAM PAGE 6 OF 7

PROGRAMMER Clément Laforce

STEP	KEY	X	Y	Z	a	b	COMMENTS
Ø2ØØ	XTO						
-	+						
-	a				i = i+1		
-	a	i					
-	UP		i				
Ø2Ø5	5	5					
-	X>Y						
-	DN	i					
-	GTO						
-	1						
Ø21Ø	9	(9)					
-	5	(95)					
-	DN	i = 5	ΣL_i				
-	DIV		b_o				
-	YTO						
Ø215	9						
-	XFR						
-	4						
-	UP	L_5	L_5				
-	+		$2L_5$				
Ø22Ø	XFR						
-	3						
-	+	L_4	$2L_5+L_4$				
-	XFR						
-	Ø		$\ldots\Sigma L_i x_i$				
Ø225	-	L_1					
-	-						
-	XFR						
-	1						
-	-	L_2					
Ø23Ø	1	1					
-	Ø	1Ø					
-	DIV		b_1				
-	3	3					
-	X		$3b_1$				
Ø235	XFR						
-	9						
-	+	b_o	L_6				Project one reading ahead.
-	1	1					
-	XTO						

REGISTERS

ØØØ	ØØ1	ØØ2	ØØ3	ØØ4	ØØ5	ØØ6	ØØ7	ØØ8	ØØ9
L_1	L_2	L_3	L_4	L_5	---	$L_o + \Delta L$	$L_o - \Delta L$	K	b_o

LEAST SQUARE PROJECTION

H·P PROGRAM FORM

TITLE STRESS RELAXATION CONTROL PROGRAM PAGE 7 OF 7

PROGRAMMER Clément Laforce

STEP	KEY	X	Y	Z	a	b	COMMENTS
0240	9						
-	S/R						
0242	END						

REGISTERS

000	001	002	003	004	005	006	007	008	009
L_1	L_2	L_3	L_4	L_5	---	$L_o + \Delta L$	$L_o - \Delta L$	K	1

APPENDIX 5: THE RATE DIAGRAMS

Following are the rate diagrams for the tests listed in Table 2.4.1; in the plots, the circles indicate experimental points and the solid lines were calculated from the equations of section 3.1.

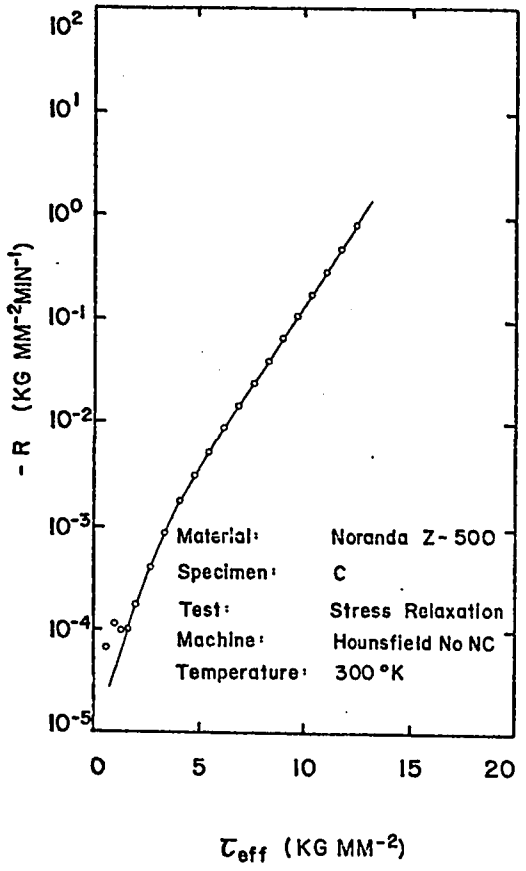
- R (KG MM⁻²MIN⁻¹)
10²
10¹
10⁰
10⁻¹
10⁻²
10⁻³
10⁻⁴
10⁻⁵
0
5
10
15
20
τeff (KG MM⁻²)
Material: Noranda Z-500
Specimen: C
Test: Stress Relaxation
Machine: Hounsfield No NC
Temperature: 300 °K

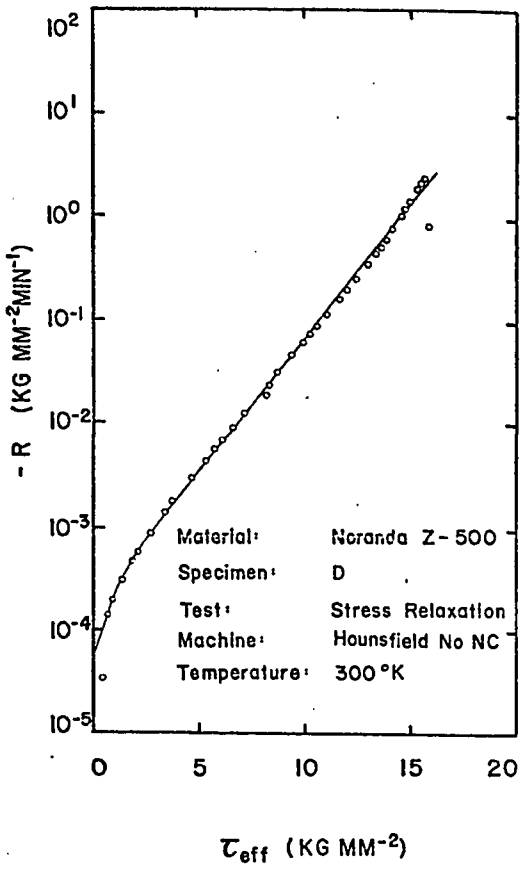
- R (KG MM⁻²MIN⁻¹)
10²
10¹
10⁰
10⁻¹
10⁻²
10⁻³
10⁻⁴
10⁻⁵
0
5
10
15
20
τeff (KG MM⁻²)
Material: Noranda Z-500
Specimen: D
Test: Stress Relaxation
Machine: Hounsfield No NC
Temperature: 300 °K

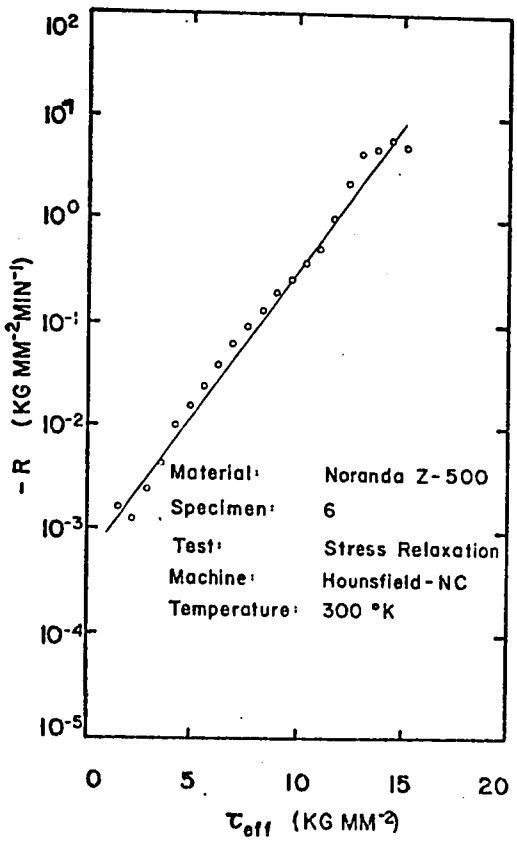
- R (KG MM⁻²MIN⁻¹)
10²
10¹
10⁰
10⁻¹
10⁻²
10⁻³
10⁻⁴
10⁻⁵
0
5
10
15
20
τeff (KG MM⁻²)
Material: Noranda Z-500
Specimen: 6
Test: Stress Relaxation
Machine: Hounsfield-NC
Temperature: 300 °K

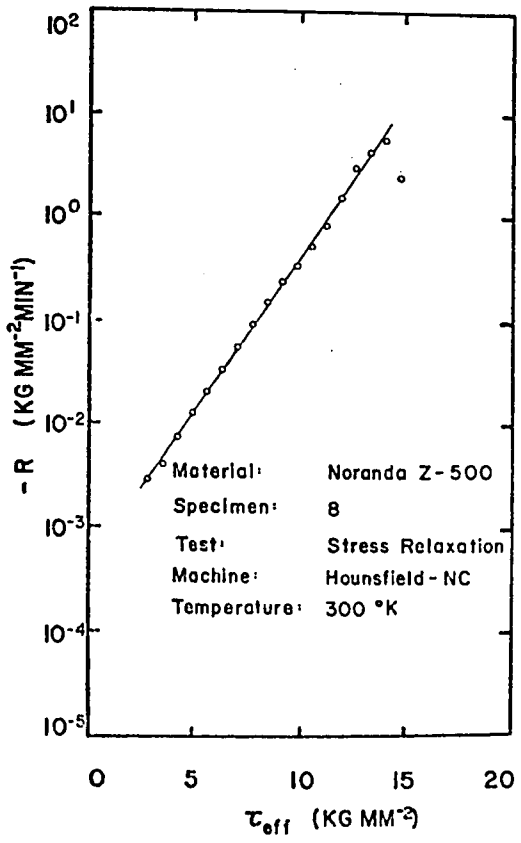
- R (KG MM⁻²MIN⁻¹)
10²
10¹
10⁰
10⁻¹
10⁻²
10⁻³
10⁻⁴
10⁻⁵
0
5
10
15
20
τeff (KG MM⁻²)
Material: Noranda Z-500
Specimen: 8
Test: Stress Relaxation
Machine: Hounsfield-NC
Temperature: 300 °K

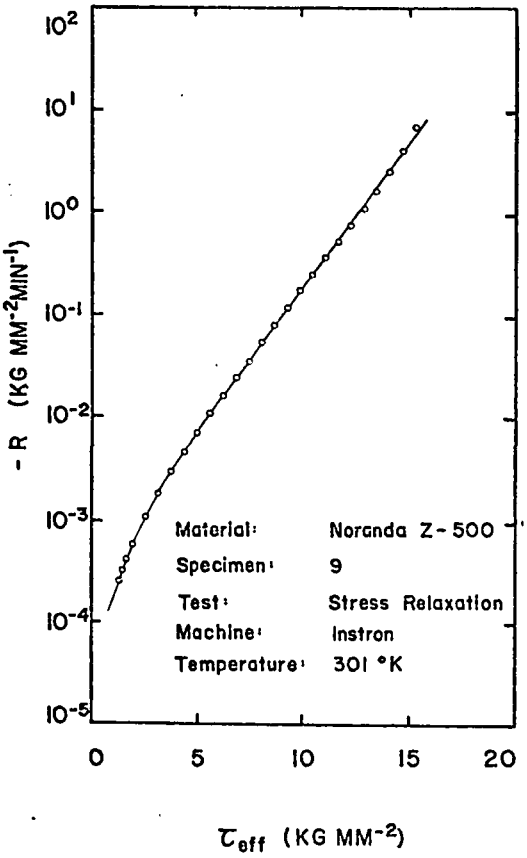
10^2
10^1
10^0
10^{-1}
10^{-2}
10^{-3}
10^{-4}
10^{-5}
- R (KG MM^{-2}MIN^{-1})
0
5
10
15
20
τ_{eff} (KG MM^{-2})
Material: Noranda Z-500
Specimen: 9
Test: Stress Relaxation
Machine: Instron
Temperature: 301 °K

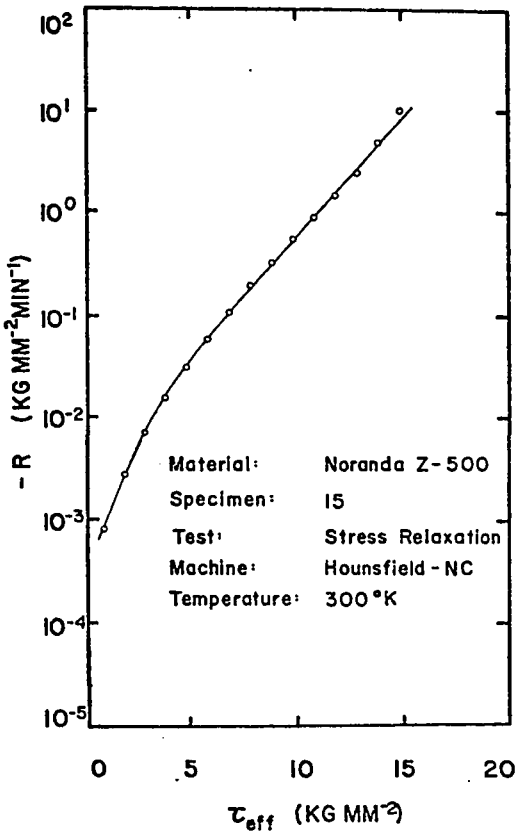
10^2
10^1
10^0
10^{-1}
10^{-2}
10^{-3}
10^{-4}
10^{-5}
- R (KG MM^{-2}MIN^{-1})
0
5
10
15
20
τ_{eff} (KG MM^{-2})
Material: Noranda Z-500
Specimen: 15
Test: Stress Relaxation
Machine: Hounsfield - NC
Temperature: 300 °K

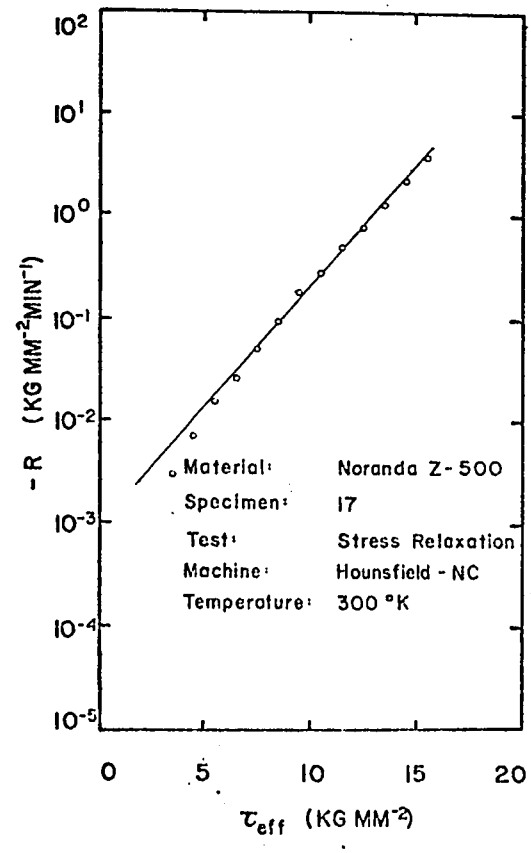
10^2
10^1
10^0
10^{-1}
10^{-2}
10^{-3}
10^{-4}
10^{-5}
- R (KG MM^{-2}MIN^{-1})
0
5
10
15
20
τ_{eff} (KG MM^{-2})
Material: Noranda Z-500
Specimen: 17
Test: Stress Relaxation
Machine: Hounsfield - NC
Temperature: 300 °K

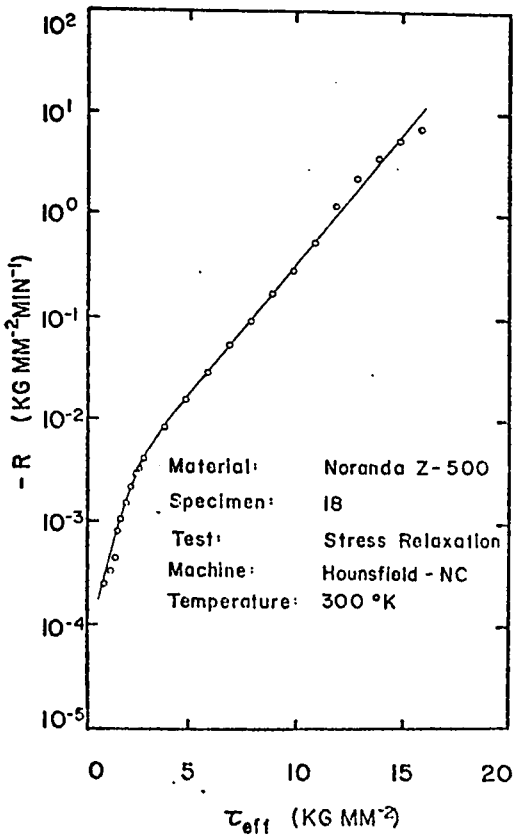
10^2
10^1
10^0
10^{-1}
10^{-2}
10^{-3}
10^{-4}
10^{-5}
- R (KG MM^{-2}MIN^{-1})
0
5
10
15
20
τ_{eff} (KG MM^{-2})
Material: Noranda Z-500
Specimen: 18
Test: Stress Relaxation
Machine: Hounsfield - NC
Temperature: 300 °K

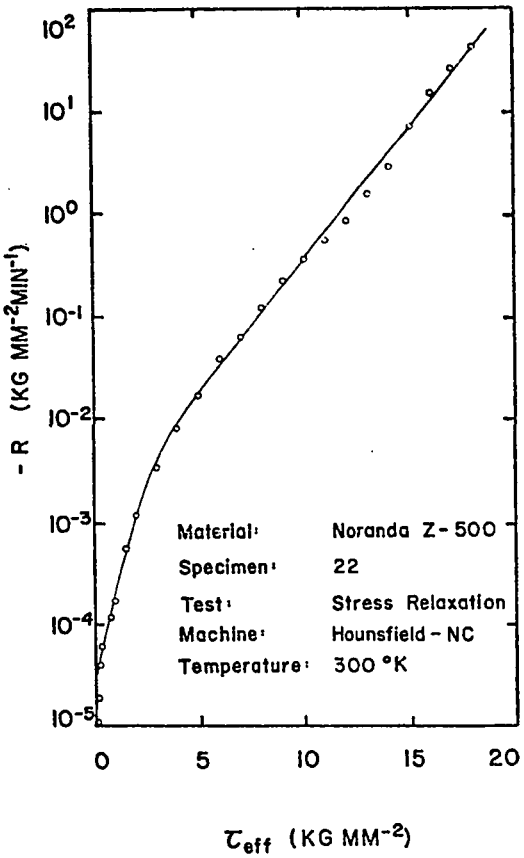
Material: Noranda Z-500
Specimen: 22
Test: Stress Relaxation
Machine: Hounsfield - NC
Temperature: 300 °K
-R (KG MM^{-2}MIN^{-1})
τ_{eff} (KG MM^{-2})

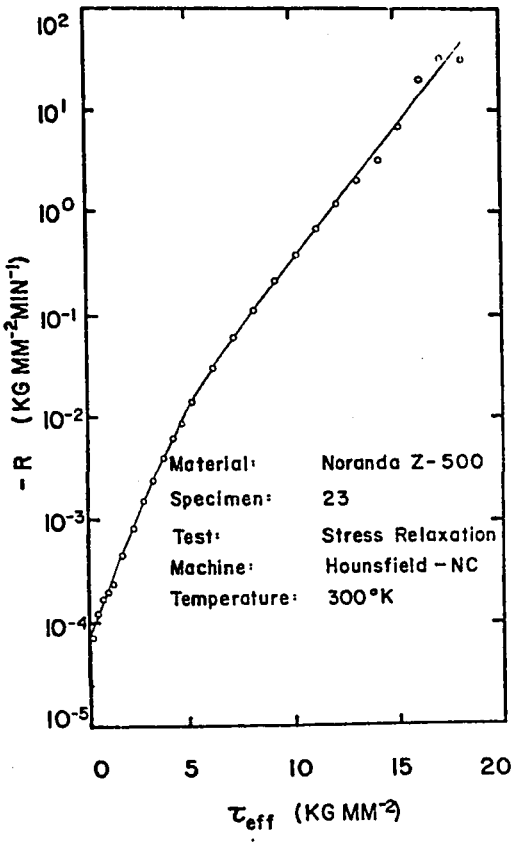
Material: Noranda Z-500
Specimen: 23
Test: Stress Relaxation
Machine: Hounsfield - NC
Temperature: 300°K
-R (KG MM^{-2}MIN^{-1})
τ_{eff} (KG MM^{-2})

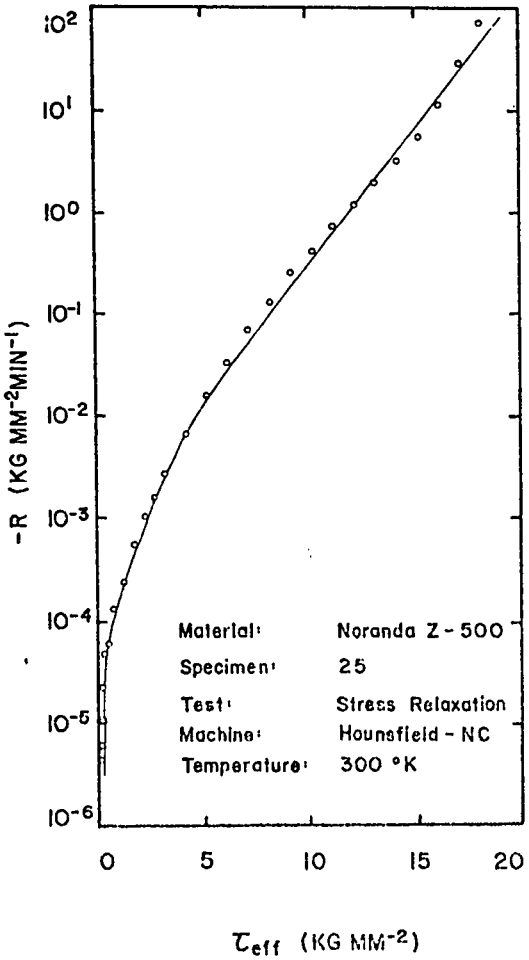
Material: Noranda Z-500
Specimen: 25
Test: Stress Relaxation
Machine: Hounsfield - NC
Temperature: 300 °K
-R (KG MM^{-2}MIN^{-1})
τ_{eff} (KG MM^{-2})

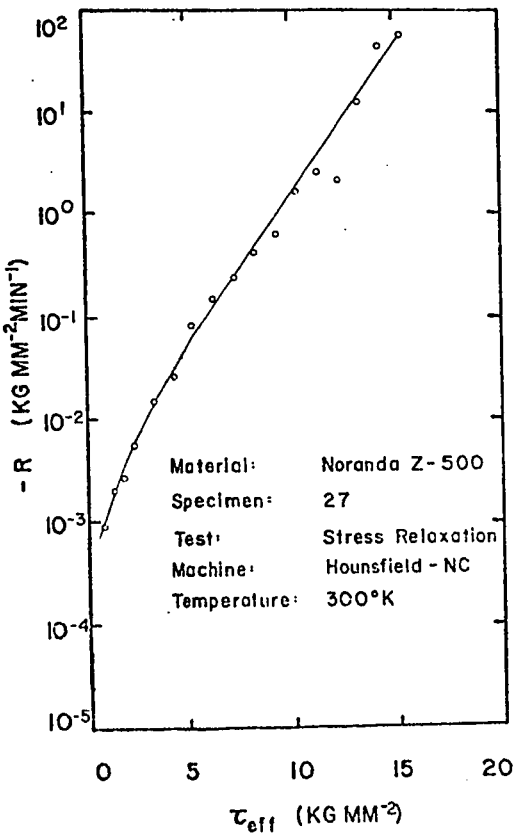
Material: Noranda Z-500
Specimen: 27
Test: Stress Relaxation
Machine: Hounsfield - NC
Temperature: 300°K
-R (KG MM^{-2}MIN^{-1})
τ_{eff} (KG MM^{-2})

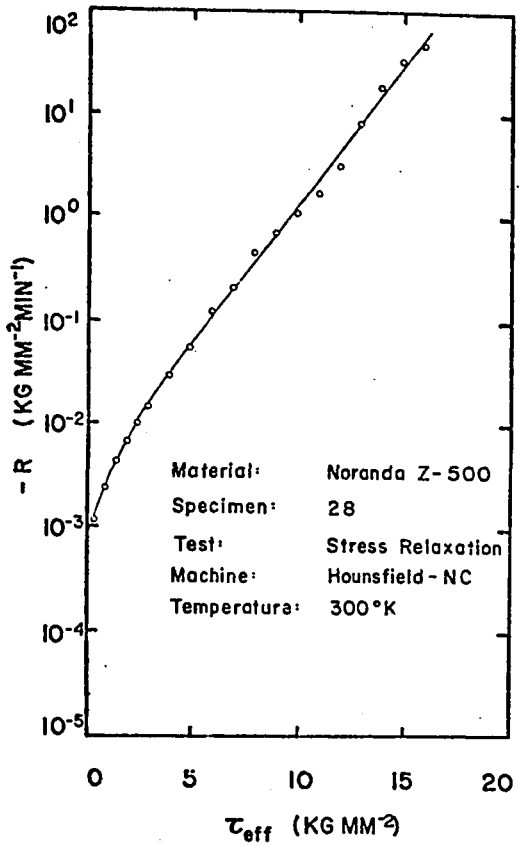
Material: Noranda Z-500
Specimen: 28
Test: Stress Relaxation
Machine: Hounsfield - NC
Temperatura: 300°K
- R (KG MM⁻²MIN⁻¹)
τeff (KG MM⁻²)

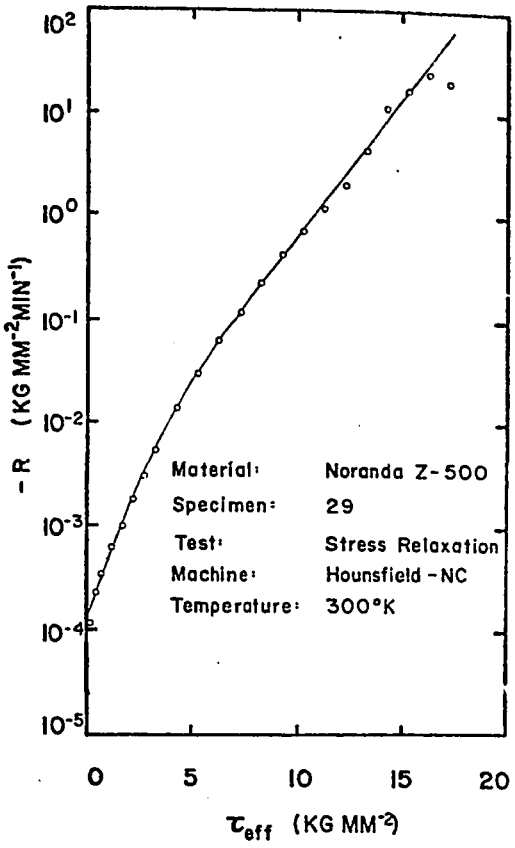
Material: Noranda Z-500
Specimen: 29
Test: Stress Relaxation
Machine: Hounsfield - NC
Temperature: 300°K
- R (KG MM⁻²MIN⁻¹)
τeff (KG MM⁻²)

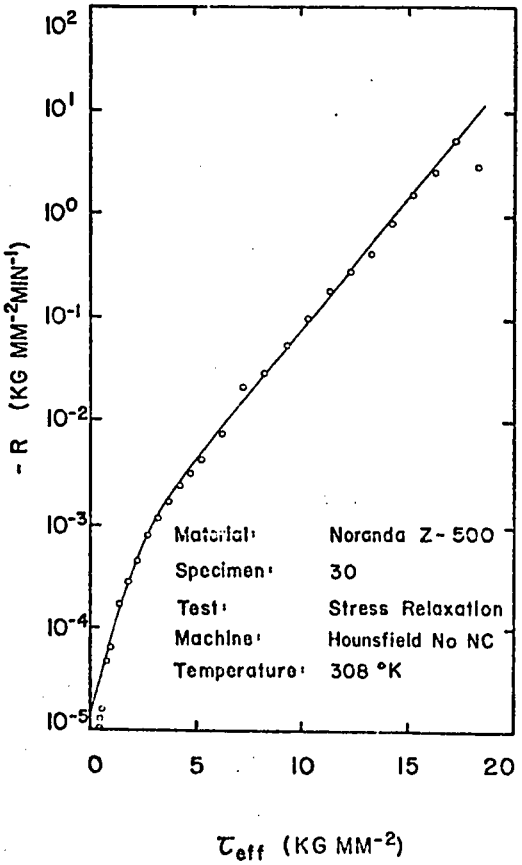
Material: Noranda Z-500
Specimen: 30
Test: Stress Relaxation
Machine: Hounsfield No NC
Temperature: 308 °K
- R (KG MM⁻²MIN⁻¹)
τeff (KG MM⁻²)

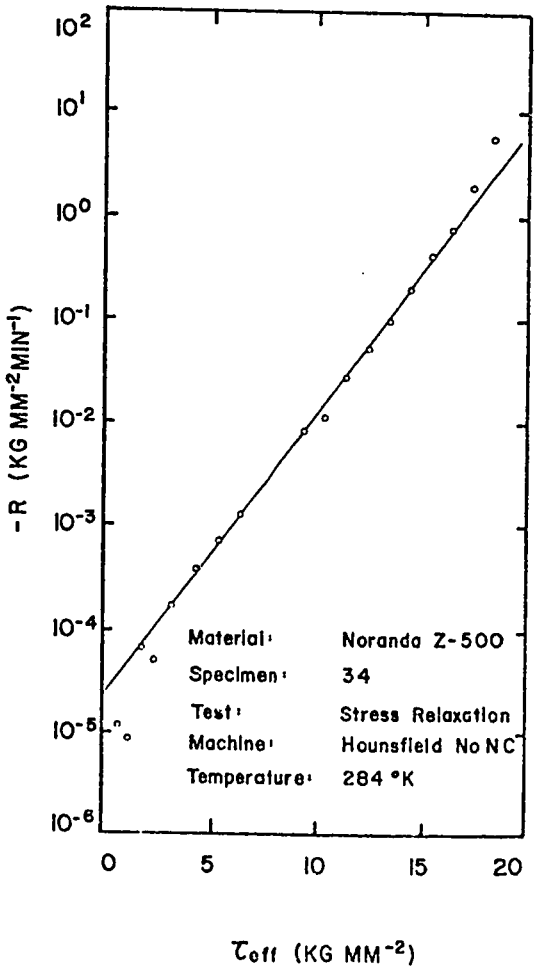
Material: Noranda Z-500
Specimen: 34
Test: Stress Relaxation
Machine: Hounsfield No NC
Temperature: 284 °K
- R (KG MM⁻²MIN⁻¹)
τeff (KG MM⁻²)

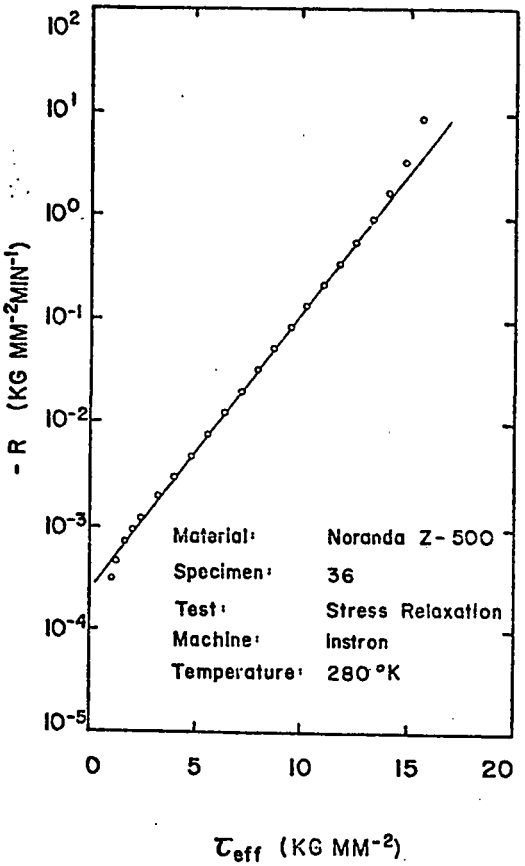
- R (KG MM⁻²MIN⁻¹)
Material: Noranda Z-500
Specimen: 36
Test: Stress Relaxation
Machine: Instron
Temperature: 280 °K
τeff (KG MM⁻²)

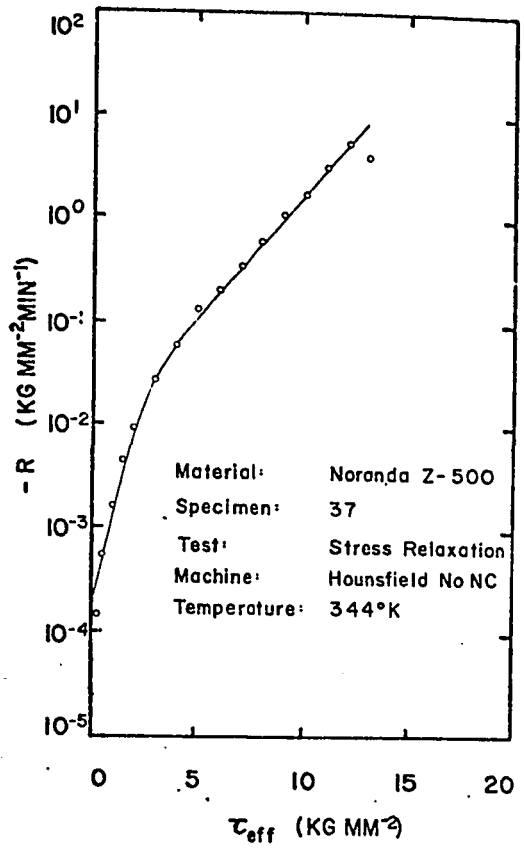
- R (KG MM⁻²MIN⁻¹)
Material: Noranda Z-500
Specimen: 37
Test: Stress Relaxation
Machine: Hounsfield No NC
Temperature: 344°K
τeff (KG MM⁻²)

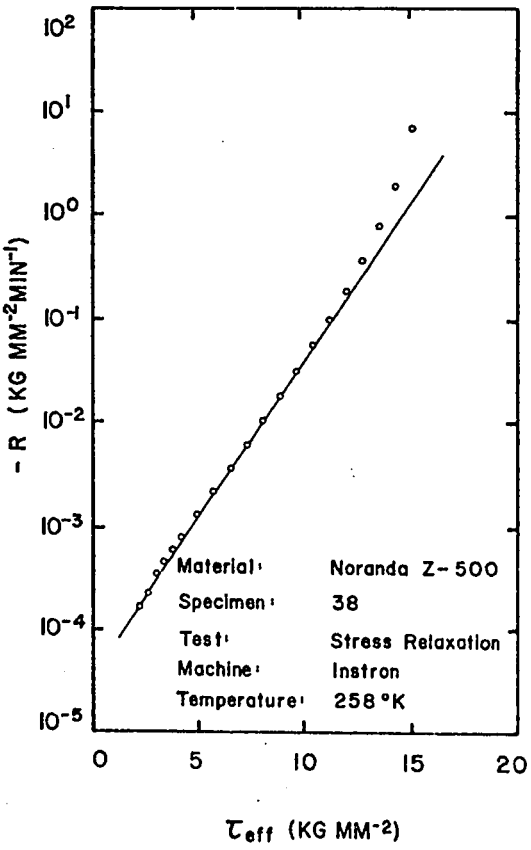
- R (KG MM⁻²MIN⁻¹)
Material: Noranda Z-500
Specimen: 38
Test: Stress Relaxation
Machine: Instron
Temperature: 258 °K
τeff (KG MM⁻²)

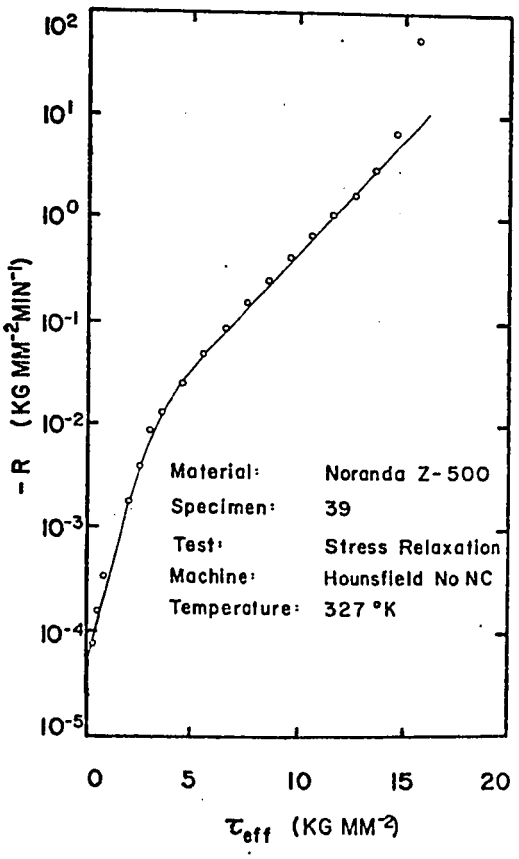
- R (KG MM⁻²MIN⁻¹)
Material: Noranda Z-500
Specimen: 39
Test: Stress Relaxation
Machine: Hounsfield No NC
Temperature: 327 °K
τeff (KG MM⁻²)

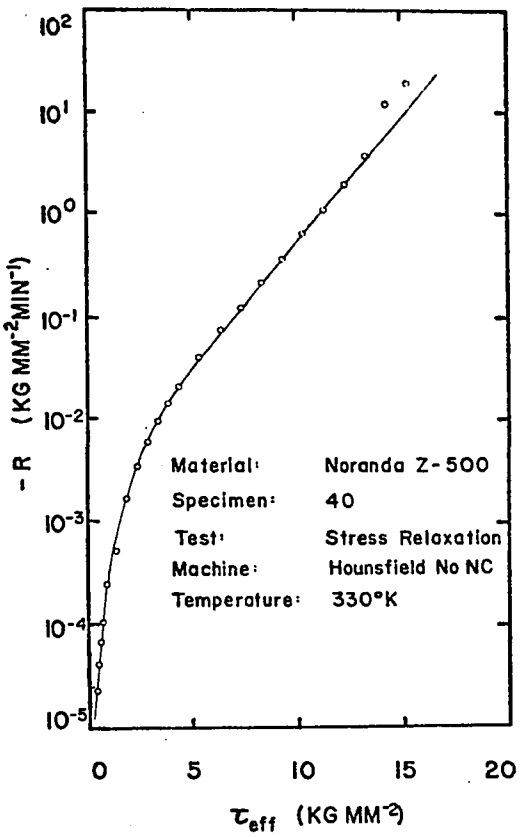
Material: Noranda Z-500
Specimen: 40
Test: Stress Relaxation
Machine: Hounsfield No NC
Temperature: 330°K
- R (KG MM⁻²MIN⁻¹)
τeff (KG MM⁻²)

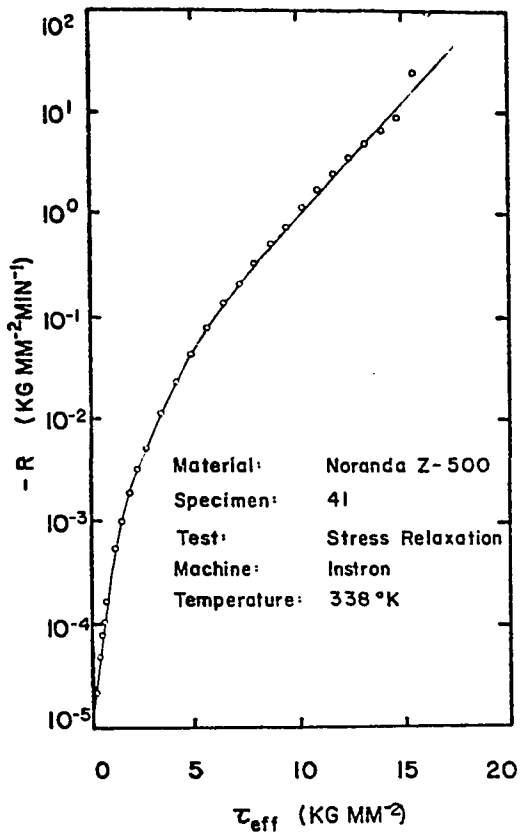
Material: Noranda Z-500
Specimen: 41
Test: Stress Relaxation
Machine: Instron
Temperature: 338 °K
- R (KG MM⁻²MIN⁻¹)
τeff (KG MM⁻²)

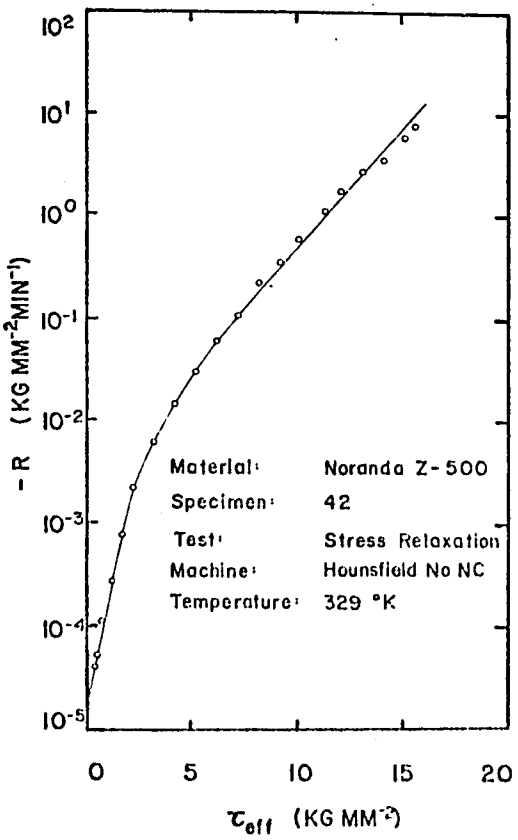
Material: Noranda Z-500
Specimen: 42
Test: Stress Relaxation
Machine: Hounsfield No NC
Temperature: 329 °K
- R (KG MM⁻²MIN⁻¹)
τeff (KG MM⁻²)

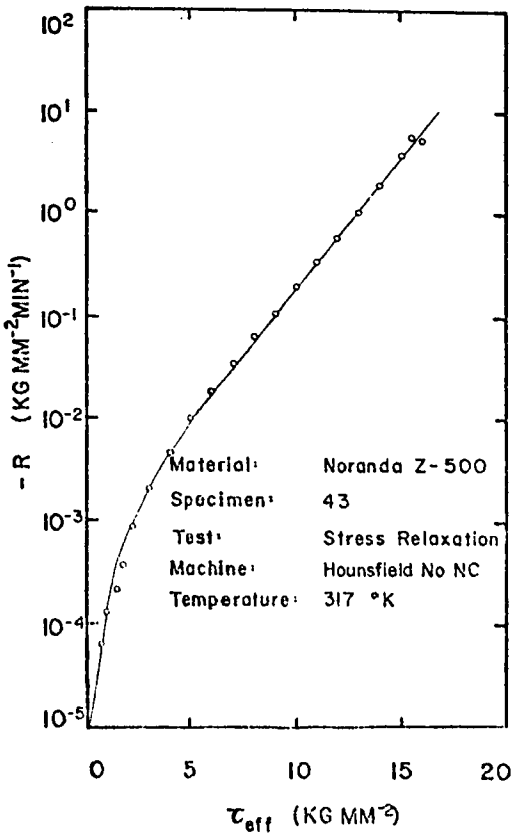
Material: Noranda Z-500
Specimen: 43
Test: Stress Relaxation
Machine: Hounsfield No NC
Temperature: 317 °K
- R (KG MM⁻²MIN⁻¹)
τeff (KG MM⁻²)

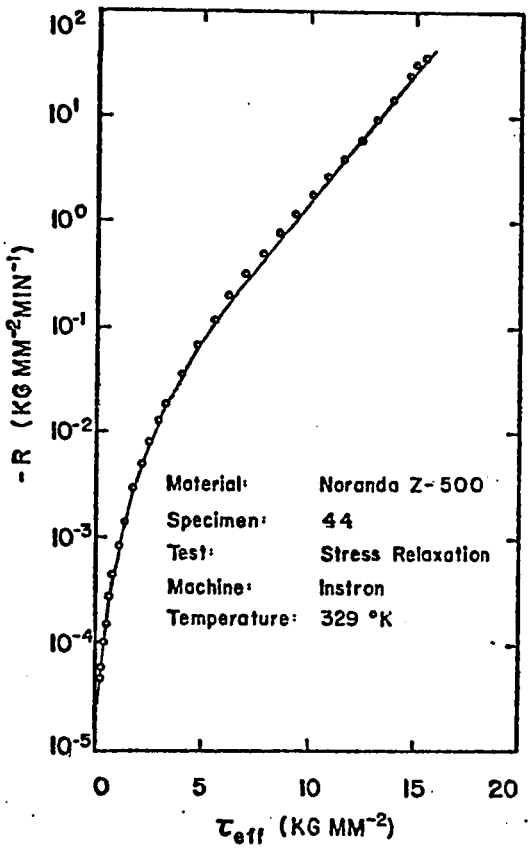
10^2
10^1
10^0
10^{-1}
10^{-2}
10^{-3}
10^{-4}
10^{-5}
$-R$ (KG MM^{-2}MIN^{-1})
0
5
10
15
20
τ_{eff} (KG MM^{-2})
Material: Noranda Z-500
Specimen: 44
Test: Stress Relaxation
Machine: Instron
Temperature: 329 °K